Ruthenium and Osmium Bis-Arene Complexes with Biologically-Active Ligands

A Thesis Submitted for the Degree of Doctor of Philosophy

by

Jennifer C. Gray, *MChem*

School of Chemistry

Faculty of Science and Engineering

University of Edinburgh

August 2008

Abstract

The inclusion of biologically-active ligands into organometallic complexes offers much scope for the design of novel drugs with enhanced, targeted activity. Studies on such complexes indicate that new mechanisms of action are possible when combining the bioactivity of the ligand with the properties inherent to the metal, leading to the possibility of overcoming current drug resistance pathways. This thesis is concerned with the synthesis and characterisation of ruthenium(II) and osmium(II) bis-arene complexes containing biologically-active ligands and their potential application as anticancer agents. Four groups of ligands are investigated: indole derivatives, aspartame, tamoxifen and flavonoids.

Both indole derivatives studied resulted in the formation of complexes which were unstable, due to either polymerisation of the ligand or decomposition of the complex as a result of loss of the bound ligand with time. X-ray structural data obtained for [(η^6-*p*-cymene)Ru(η^6-1-methylindole-3-acetic acid)]$(PF_6)_2$ revealed that the latter may be a result of partial loss of η^6-coordination due to tilting of the indole ring away from the metal.

Much more stable complexes were generated with aspartame, however the effect of the metal on the structure, electronics, acidity and decomposition of the ligand all resulted in the complexes being incapable of binding to and activating the human sweet taste receptor.

Antiproliferative studies found that ruthenium and osmium complexes of tamoxifen were not active against hormone-dependent mcf-7 breast cancer cells although they were able to mimic the isolated ligand under certain conditions. Here, the inactivity

is most likely a result of the organometallic fragment being too bulky to fit into the receptor active site. Although no cytotoxic activity was observed, evidence of intercalation of the complexes into DNA was obtained.

Dual anticancer activity was discovered for two ruthenium complexes of flavonoids: $[(\eta^6\text{-}p\text{-cymene})Ru(\eta^6\text{-flavanone})](PF_6)_2$ and $[(\eta^6\text{-biphenyl})Ru(\eta^6\text{-flavanone})](PF_6)_2$. Although the complexes are very similar in structure, the first displayed moderate cytotoxic activity against both A2780 and A549 cancer cells (IC_{50} 30 – 40 μM), which may be a result of an observed DNA interaction, while the second was selectively highly cytotoxic towards A549 cancer cells (IC_{50} ~ 6 μM) and showed no evidence of targeting DNA. Moreover, antioxidant properties inherent to the ligands were found to be enhanced on metal binding, giving the complexes additional potential in applications for the prevention of cancer.

Significantly, this work has identified the first anticancer active metal bis-arene complexes of biologically-active ligands, therefore demonstrating the validity of such an approach to the design of novel drugs.

Declaration

I hereby declare that except where specific reference is made to other sources, the work contained in this thesis is the original work of the author. It has been composed by myself and has not been submitted, in whole or in part, for any other degree, diploma, or other qualification.

Jennifer Gray

August 2008

Acknowledgements

I would like to thank Professor Peter J. Sadler for his supervision and encouragement throughout my project. I have gained a lot of invaluable knowledge from him over the past three years and it has been a pleasure working in his group.

Thanks to Dr. Marcel Winnig and Professor Wolfgang Meyerhof for their collaboration on the aspartame complexes and for performing the sweet taste receptor assays. I would also like to thank Dr. Euan Murray and Professor Ted Hupp at the University of Edinburgh Cancer Research Centre for their help with the biological assays performed on the tamoxifen complexes. Thanks also go to Mr. Daniel Cole and colleagues at Oncosence Ltd for testing the cytotoxicity of several of the ruthenium complexes reported in this thesis and to Professor Viktor Brabec and co-workers for data on the DNA interactions of the flavonoid complexes. I am very grateful to Mr. Juraj Bella and Mr. John Miller for their help with NMR and to Professor Simon Parsons and his research group for solving the crystal structures reported in this thesis.

For financial support with this project I would like to thank the EPSRC. I would also like to thank the University of Edinburgh Chemistry Department and The Royal Society of Chemistry for financial assistance, allowing me to present my work at a number of conferences.

A big thank you goes to all members, both past and present, of the Sadler group, with whom I have formed many friendships. A special thank you goes to Dr. Abraha Habtemariam, not only for his assistance with getting my project started but also for his continued support and guidance throughout my PhD. Thanks also to Dr. Anna

Peacock and Dr. Sarah Dougan for all their advice on the project and to Miss Tijana Bugarcic for performing the energy minimisation calculations.

A final thank you goes to all my family for their eternal support and to Ross for his patience and encourgament over the last three years, especially in the final months whilst I have been writing up.

Contents

Abbreviations

δ	chemical shift (NMR)
λ	wavelength
η^6	eta-6 coordination
AgOTf	silver trifluoromethanesulfonate
$AgPF_6$	silver hexafluorophosphate
Anal.	analysis
ca.	circa (about)
CD	circular dichroism
CHN	carbon, hydrogen, nitrogen (elemental analysis)
cisplatin	*cis* – $[PtCl_2(NH_3)_2]$
COSY	correlation spectroscopy
Cp	$\eta^5 - C_5H_5$
d	doublet
Dc	calculated density
dd	doublet of doublets
DMF	dimethylformamide
DMSO	dimethylsulfoxide
DNA	deoxyribonucleic acid
EtBr	ethidium bromide ($C_{21}H_{20}BrN_3$)
ESI-MS	electrospray ionisation mass spectrometry
HPLC	high performance liquid chromatography
HSQC	heteronuclear spin-quantum coupling spectroscopy
IC_{50}	50% growth inhibition concentration
K	Kelvin

m	multiplet
[M]	molecular ion (MS)
MeOD	methanol-d_4
mol equiv	molar equivalent
m/z	mass/charge
NMR	nuclear magnetic resonance
NOESY	nuclear overhauser effect spectroscopy
OTf	triflate (CF_3SO_3)
p-cymene	*para*-cymene
ppm	parts per million
s	singlet / seconds
sp	septet
t	triplet
TFA	trifluroacetic acid
TOCSY	total correlation spectroscopy
U	volume of cell
Z	number of asymmetric units per cell

Chapter 1 Introduction

1.1 Introduction

This thesis is concerned with the synthesis and characterisation of ruthenium(II) and osmium(II) bis-arene complexes containing biologically-active ligands and their potential application as anticancer agents. A strong focus of this work involves investigating and understanding modifications to the ligand's properties on metal binding, with a view to obtaining a greater chemical knowledge of such systems. This Chapter discusses metal-based drugs, previous work in the area of metal complexes of bioactive ligands, the comparative chemistries of ruthenium and osmium and the prospective biological interactions of metal bis-arene complexes.

1.2 Metal-based Drugs

Metal ions are often classed as 'toxic' or 'non-toxic', however their biological activity depends very much on speciation and it is now widely accepted that, with carefully controlled coordination chemistry, even 'toxic' metals can exhibit therapeutic properties[1]. It is also true that toxicity is concentration-dependent and elements considered to be biologically essential can be toxic at high doses (Bertrand Diagram[2], Figure 1.1). It is therefore very important to investigate and understand the effects of varying the oxidation state, numbers and geometries of coordinated ligands on the biological properties of metal complexes to design metal-based drugs with therapeutic properties at desired doses successfully[3].

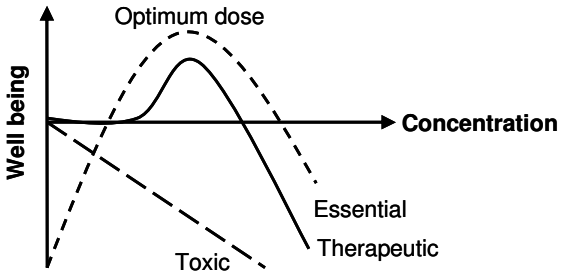

Figure 1.1 The Bertrand Diagram[2] representing the relationship between the therapeutic benefit of an element and its concentration.

A number of metallic elements play crucial roles in biology and it is clear that many organic compounds used in medicine require metal ions for activation or biotransformation in order to achieve their mode of action. For example, haemoglobin which binds and delivers oxygen to body tissues requires an iron atom to function and calcium minerals are required in order for our bones to exist and grow. Electron-deficient metal centres attract electron rich biomolecules, such as proteins or DNA, leading to a high tendency for metal ions to bind to and interact with important biological targets. It is this extensive use of metal ions by nature which prompted inorganic chemists to investigate the potential of utilising metal complexes in medicinal applications[4].

Although research into metal-based drugs only began in the early 1900s, metal compounds have been used in medicine for thousands of years. The ancient Egyptians used copper to sterilise water, medicines containing gold were taken in China and Arabia around 2500 BC and zinc was used to aid the healing of wounds around 1500 BC[5]. However, it was the discovery of the anticancer activity of

cisplatin [*cis*-$PtCl_2(NH_3)_2$] (Figure 1.2) by Barnett Rosenberg in the 1960s, which remains the world's highest selling anticancer drug, that stimulated research into inorganic medicinal chemistry worldwide[5]. Since then, the versatility of metal-based drugs has been illustrated by the design of a vast number of complexes for a wide range of therapeutic applications. For example; sodium nitroprusside is an iron-based cardiovascular drug, the gold complex auranofin is used in the treatment of arthritis, silvadene (silver sulfadiazine) has antibacterial and antifungal properties and is used in the treatment of burns, bis(maltato)oxovanadium (BMOV) is an orally active insulin mimetic used to treat diabetes and Ceretec is a ^{99m}Tc(V) complex used as an imaging agent (Figure 1.2)[6].

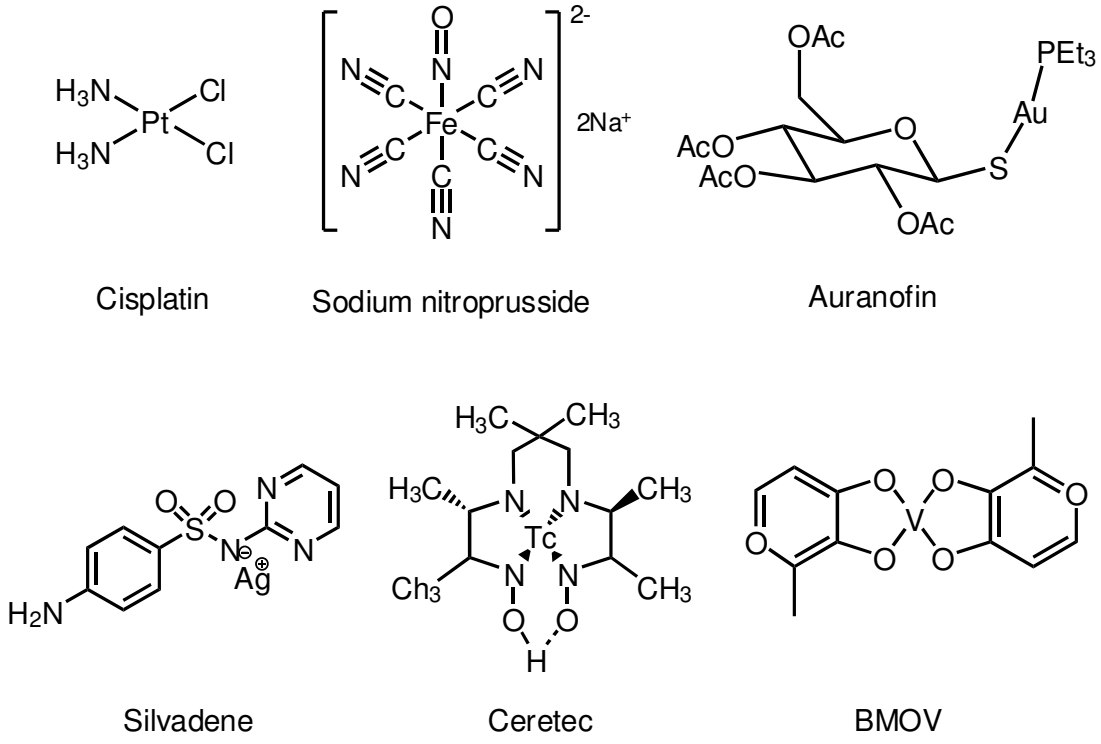

Figure 1.2 Examples of metal-based drugs. The platinum anticancer drug cisplatin, sodium nitroprusside, auranofin, silvadene, BMOV and Ceretec.

1.3 Metal Anticancer Agents

As illustrated in Section 1.2, metal complexes have a broad range of medicinal applications. Since those described in this thesis are assessed primarily for their potential to act as anticancer agents, a more detailed discussion of previous work in this area is presented.

Cancer is a major cause of death worldwide[7]. It is the term used to describe over 200 diseases which possess the common characteristic of uncontrolled cell division and the ability of these cells to invade healthy tissue. There are many approaches to the treatment of cancer depending on the form and stage of the disease, however there is a constant need for research into new drugs with novel mechanisms of action[7].

Following the discovery of cisplatin in 1969, there has been a vast expansion of research into the use of inorganic compounds in the treatment of cancer. Despite its success in the treatment of a wide range of cancers, cisplatin has a number of drawbacks which include toxicity and resistance[8]. This has led to the development of 2nd generation platinum drugs, such as carboplatin and oxaliplatin[9], which were found to have lower toxicity and are currently used for the treatment of ovarian and colon cancer, respectively[10]. Third generation compounds are also being explored, including the first orally active platinum drug, satraplatin (Figure 1.3), which is reduced *in vivo* and is currently undergoing clinical trials[11].

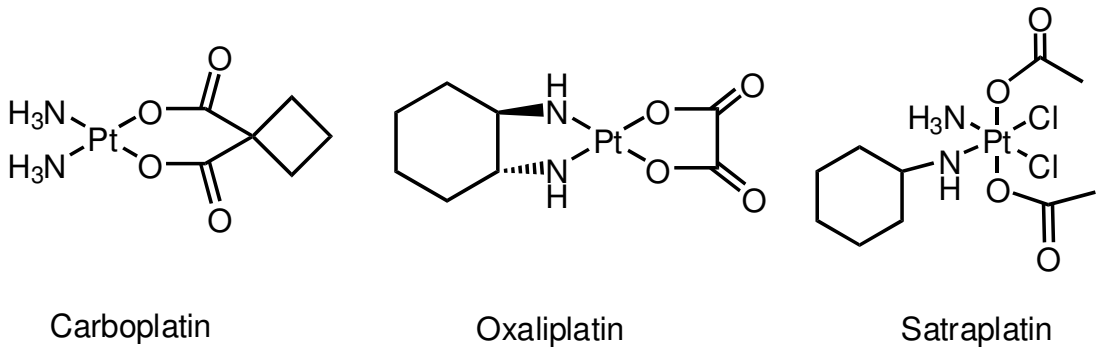

Carboplatin Oxaliplatin Satraplatin

Figure 1.3 The chemical structures of the 2nd generation platinum anticancer agents carboplatin and oxaliplatin and the 3rd generation orally active drug satraplatin.

There is also emerging literature regarding the use of non-toxic photoactivatable platinum(IV) complexes as pro-drugs which are activated by light to generate toxic platinum(II) species selectively at the target tumour site, thus reducing toxic side-effects[12, 13]. Such complexes are currently being developed in research labs, two examples of which are shown in Figure 1.4. Both were found to be non-toxic (IC_{50} value greater than 300 μM) to 5637 bladder cancer cells in the dark but when irradiated with light their toxicity dramatically increased with IC_{50} values of 49 and 63 μM for *cis,trans,cis*-$[Pt(N_3)_2(OH)_2(NH_3)_2]$ and *cis,trans*-$[Pt(N_3)_2(OH)_2(en)]$, respectively (IC_{50} value = concentration of drug required to inhibit growth of cells by 50%). They have also been shown to be active against a cisplatin-resistant cell line, indicating that the mechanism by which they kill cancer cells is different from that of cisplatin[1].

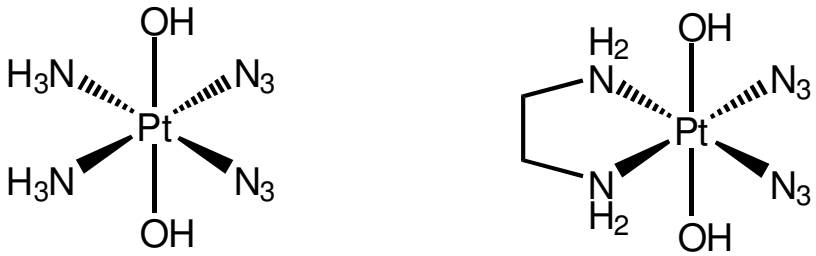

Figure 1.4 The chemical structures of *cis,trans,cis*-[$Pt(N_3)_2(OH)_2(NH_3)_2$] and *cis,trans*-[$Pt(N_3)_2(OH)_2$(en)], two photoactive platinum(IV) complexes which, on irradiation with light, become toxic to cells through generation of highly reactive platinum(II) species[1].

Ruthenium complexes have also received a lot of interest and are now studied intensively for their anticancer properties[14]. Ruthenium was seen as a promising metal due to its similar kinetics to platinum, on timescales comparable to cellular division processes[11], and its lower toxicity thought to be due to its ability to mimic iron and therefore bind to biomolecules such as serum albumin and transferrin[15]. Anticancer activity for ruthenium(III) complexes was first reported for Ru(III) ammines by Clarke, however they were too insoluble for use in the clinic[1]. Since then, two of the most promising Ru(III) complexes are *trans*-tetrachlorodimethylsulfoxideimidazoleruthenate(III) (NAMI-A) and *trans*-tetrachlorobis(1H-indazole)ruthenate(III) (KP-1019) which have both entered clinical trials[16]. It is thought that such Ru(III) complexes act as prodrugs and are activated by reduction to Ru(II) *in vivo* to generate more labile complexes which can coordinate rapidly to biomolecules[14]. This led to increased efforts to study ruthenium(II) complexes, and of particular relevance to the work described in this thesis are the active organometallic ruthenium(II) mono-arene complexes.

Complexes of this type can be fine-tuned by varying the ligands to obtain desired pharmacological properties[17]. For example, $[(\eta^6\text{-THA})Ru(en)Cl]^+$ where THA = tetrahydroanthracene and en = ethylenediamine (Figure 1.5) has activity comparable to cisplatin with an IC_{50} value of 0.5 μM against A2780 human ovarian cancer cells (cisplatin IC_{50} = 0.6 μM)[18]. It is interesting to note that osmium-arene analogues have also been investigated recently with some showing high *in vitro* cytotoxicity[19].

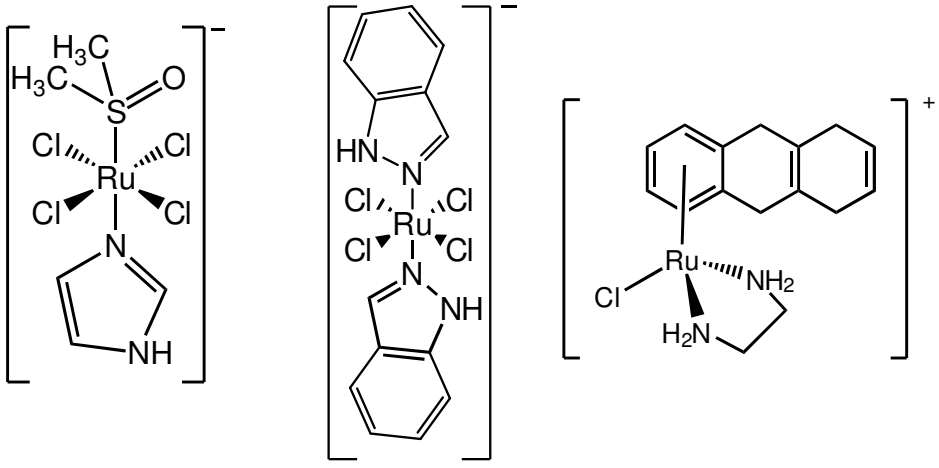

NAMI-A KP1019 $[(\eta^6\text{-THA})Ru(en)Cl]^+$

Figure 1.5 The chemical structures of NAMI-A, KP1019 and $[(\eta^6\text{-THA})Ru(en)Cl]^+$.

Although platinum and ruthenium have received the most interest in this area of research, it should be noted that many other metals have also been explored and some examples of these are shown in Figure 1.6[20, 21].

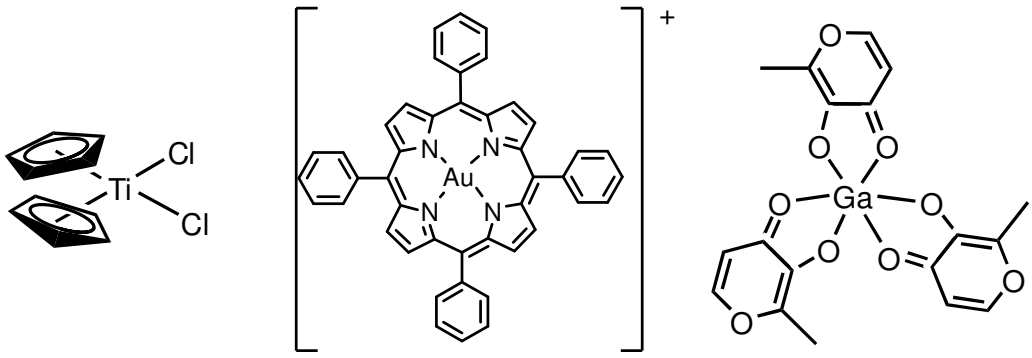

Figure 1.6 The chemical structures of other metal complexes investigated for their potential as anticancer agents: titanocene dichloride, gold tetraphenylporphyrin and gallium maltolate.

1.4 Metal Complexes of Biologically-Active Ligands

In recent years, research into new pharmaceuticals, both organic and inorganic, has seen a change in trend away from cytotoxic compounds to molecular targeting agents[5]. This is particularly true for the treatment of cancer as there is a constant strive to overcome drug resistance by opening up new mechanisms of action[22].

One approach which has shown rapid growth in recent years and a number of notable successes is the design of metal complexes incorporating biologically active ligands. Such compounds offer the possibility for design of metal-based drugs with enhanced, targeted activity by combining the specificity of the ligand to interact with a particular molecular site with the properties inherent to the metal centre. Consequently, there is a huge scope for design, attributable to the choice of metals available and the range of accessible oxidation states, number and type of additional coordinating ligands. This is turn allows the kinetics and thermodynamics of the complex to be controlled to a certain extent[23]. It is also true that the presence of the

metal could result in more efficient delivery of the active ligand to the target as the solubility, biodistribution and pharmacokinetics may be dramatically altered[22].

There are many examples of such complexes in the literature, incorporating a wide variety of biologically-active ligands such as amino acids[24], hormones[25], antimalarial drugs[26], inhibitors of resistance pathways[27] and non-steroidal anti-inflammatory drugs[22] and with applications ranging from immunoassay tracers[25] to small molecule delivery agents[22]. There are also a number of non-medicinal applications such as catalysis and 'supports' for peptide synthesis[24]. A number of promising compounds in the field of cancer research have also been identified. These include cobalt complexes of nitrogen mustards, which show a 20-fold preference for hypoxic cancer cells over healthy cells[22] and perhaps most significantly, and of particular relevance to this work due to their organometallic nature, the Ferrocifen series of complexes (Figure 1.7) of the breast cancer drug tamoxifen. By replacing the phenyl group for a ferrocenyl centre, activity was found against both hormone independent and dependent breast cancer cells whereas tamoxifen is only active against the latter. These will be discussed in more detail in Chapter 5.

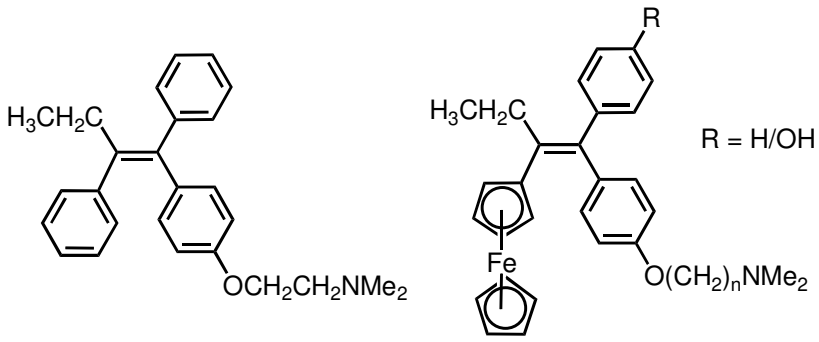

Figure 1.7 The organometallic Ferrocifen series of complexes (right) derived from the purely organic breast cancer drug tamoxifen (left).

1.5 Chemistry of Ruthenium and Osmium

This thesis is concerned with organometallic complexes of ruthenium and osmium, therefore their comparative chemistries are briefly discussed.

1.5.1 General

Ruthenium and osmium are both group 8 transition metals positioned in the second and third row of the periodic table, respectively. They belong to a collection of metals classified as the 'Platinum group', which also consists of rhodium, palladium, iridium and platinum. All these metals have closely related physical and chemical properties and often occur together in the same mineral deposits. Osmium was discovered 41 years before its second row analogue, however much less is known about its chemistry[28]. This is most likely due to the higher cost of the metal and the greater difficulty associated with compound synthesis[29].

The two most common oxidation states of ruthenium, Ru(II) and Ru(III), are both substitutionally inert, although the latter to a greater extent. This makes ruthenium unique within the periodic table and is a feature which has proved useful for a number of single-electron transfer studies[30]. Third row transition metals are commonly more inert than those in the second and first rows and consistent with this, osmium is more inert than ruthenium, with ligand exchange rates around 10^5 times slower[31]. As a result of the lanthanide contraction, osmium is very similar in size to ruthenium, however due to its position in the third row, its outer 5d orbitals are highly exposed and hence sensitive to the electronic nature of coordinating ligands.

Although osmium is found in a wider range of oxidation states than ruthenium (-2 to +8 compared to 0 to +8), this does not extend to coordination number. Apart from the most well-known osmium complex, osmium tetroxide (OsO_4), the majority of complexes are low-spin octahedral[28]. In contrast to both ruthenium and iron, no characteristic cationic aqua ion $[M(OH_2)_6]^{3+/2+}$ species has been detected for osmium[31].

1.5.2 Ruthenium and Osmium in Medicine

As discussed in Section 1.3, ruthenium compounds are suitable for use in biological applications due to their slow ligand exchange rates which are close to those of cellular processes and the capability of the metal to mimic iron in binding to specific biological molecules. An additional feature is that the oxidation states Ru(II), Ru(III) and Ru(IV) are accessible under physiological conditions, with reductants such as glutathione and ascorbate being capable of reducing Ru(III) and Ru(IV) and the

oxidation of Ru(II) readily induced by molecular oxygen or cytochrome oxidase[15]. The cytological stain, Ruthenium Red, $[(NH_3)_5Ru\text{-}O\text{-}Ru(NH_3)_4\text{-}O\text{-}Ru(NH_3)_5]^{6+}$, was the first compound of this metal to be used in biology[14]. Since then, numerous medicinal properties of the metal have been discovered including antimalarial, antimicrobial and anticancer, of which the latter has been covered in more detail in Section 1.3[15]. Furthermore, the radioactive nucleotide of ruthenium (^{97}Ru) has shown promise as a radiopharmaceutical, with advantages over the currently widely used technetium alternative (^{99m}Tc) due to its longer half life allowing for more manipulation prior to use; however there are problems due to its lack of commercial availability[14].

Medicinal applications of osmium are much less common because it is generally not considered to be biologically relevant and in some forms can be highly toxic. However, some osmium complexes have been used for the treatment of rheumatoid arthritis in animals and anticancer activity has been reported for some Os(III) and Os(IV) neutral complexes[32, 33]. In addition, trypanocidal activity against *T. b. brucei* has been reported[34].

1.5.3 Organometallic Complexes

Organometallic complexes of ruthenium and osmium are most common in lower oxidation states and contain ligands ranging from arenes, allyls and cyclopentadienyls to carbonyl, nitrido and cyano groups[29, 35, 36]. Since arene complexes form the basis of this research their chemistry will be briefly covered.

Ruthenium and osmium arene complexes exist as either mono- or bis-arene structures, commonly with the metal in either the zero or +2 oxidation state[29, 35].

1.5.3.1 Mono-Arene Complexes

Ruthenium(II) and osmium(II) mono-arene complexes are known as 'half-sandwich' compounds with a pseudo octahedral 'piano-stool' structure, as shown in Figure 1.8[37]. The η^6-arene occupies three coordination sites (the 'seat'), with the other ligands (X, Y and Z) at the remaining sites (the 'legs')[38]. These complexes possess stable metal-arene bonds, resulting in reduced tendency to oxidise to the +3 oxidation state[39, 40]. Due to the similarity in size of the two metals, the structures of mono-arene complexes of osmium have been found to be very close to those of the ruthenium analogues with many bond lengths identical, however their chemistries have been shown to vary considerably[19, 41]. As a result of the interest in this class of complexes as anticancer drugs, extensive investigations[17, 19] into the effect of varying the arene[18, 38] and X[42, 43], Y, and Z[44-46] on the properties of the complexes have illustrated the extent to which exchange rates, structures, redox behaviour[47], solution-[48]and bio-chemistry[49, 50] are dependent on the ligands. The knowledge gained has allowed the design of complexes for specific applications. Although reports of the aqueous chemistry of Os(II) arene complexes are much more limited than for Ru(II)[19, 40], good solubility is generally observed for both metals[37, 39]. This is naturally dependent on the ligands involved and may become important in terms of tuning complexes for clinical applications.

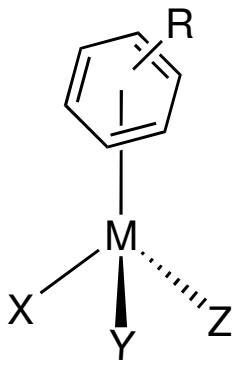

Figure 1.8 The general chemical structure of a half-sandwich metal mono-arene complex (M = Ru/Os). In applications as anticancer agents X is most often a halide and Y,Z is generally a chelating group with NN, NO or OO donor atoms.

Ru(II) and Os(II) mono-arene structures with three non-equivalent ligands possess chirality, with a stereogenic centre at the metal. This gives rise to potential applications as asymmetric catalysts for a range of reactions, including alkene hydrogenation, Diels-Alder reactions and alkene metathesis[51, 52].

1.5.3.2 Bis-Arene Complexes

Bis-arene Ru(II) and Os(II) sandwich complexes of the type shown in Figure 1.9, on which the work discussed in this thesis is based, may be synthesised from the appropriate chloride-bridged dimer, $[(\eta^6\text{-arene})MCl_2]_2$ (M = Ru/Os), by reaction with a silver salt in acetone (to remove bound chloride ligands) affording a mono-arene acetone intermediate. Reaction with a second arene in trifluoroacetic acid (TFA) yields the bis-arene structure[53, 54]. As for mono-arene complexes, bis-arene complexes are more highly documented for ruthenium. A search of the Cambridge crystallographic database (CCDC) revealed that while there are over 50 X-ray crystal

structures of ruthenium bis-arene complexes, only 2 such osmium structures have been reported. The stark contrast between these numbers and those for mono-arene complexes of ruthenium and osmium, of *ca.* 1600 and *ca.* 110 respectively, clearly indicates the limited research to date on bis-arene complexes of these metals.

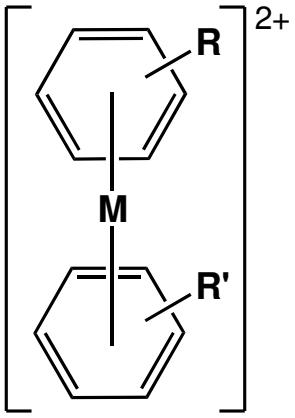

Figure 1.9 The general chemical structure of a metal bis-arene complex (M = Ru/Os)

1.5.3.3 Complexes with Bioactive Ligands

Mono-arene complexes of ruthenium and osmium containing biologically-active ligands are known most frequently for amino acids and peptides where coordination to the metal is through σ-bonding *via* functional donor group atoms[24]. Bis-arene complexes are less common and significantly, there are no reported osmium bis-arene complexes of biologically-active ligands. Nevertheless, there are a number of ruthenium examples including complexes of the essential amino acid phenylalanine[55] and derivatives of dopamine, a neurotransmitter which is important

in the regulation of many internal pathways[53] (Figure 1.10). Importantly, the biologically activity of such complexes has not been investigated to date.

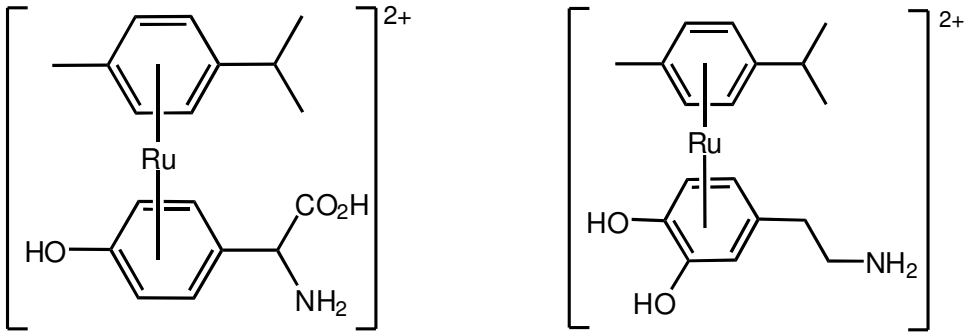

Figure 1.10 The chemical structures of [(η^6-*p*-cymene)Ru(η^6-phenylalanine)]$^{2+}$ [55] (left) and [(η^6-*p*-cymene)Ru(η^6-H-dopamine)]$^{2+}$ [53] (right).

1.6 Prospective Biological Interactions of Metal Bis-arene Complexes

Metal complexes with the structures studied in this thesis have received very limited attention for potential applications as anticancer agents, although some work has been done which found them to possess good activity[56, 57]. In addition to the interesting properties the presence of the bioactive ligand will bring in the complexes studied in this thesis, a number of prospective biological interactions may be identified based on the physical and chemical properties of known metal bis-arene structures. Two such interactions which could lead to cytotoxicity to cancer cells are briefly discussed here to further illustrate the stimulation behind the research described in this thesis.

1.6.1 Accumulation in Mitochondria

Mitochondria are central to cell function. They are involved in many processes such as; ATP synthesis, calcium uptake and release, pH control and DNA synthesis[58]. They are also considered to play a fundamental role in the regulation of programmed cell death (apoptosis)[59]. In response to certain stimuli, the outer membrane of the mitochondria becomes permeable, permitting soluble proteins such as cytochrome *c* to translocate to the intracellular region of the cell. These proteins are thought to activate caspases (signal transducing molecules) which in turn trigger cell death[59]. Mitochondria have been identified as important targets for the treatment of cancer[60], neurodegenerative diseases[61] and diabetes[62]. The targeting of mitochondria for the treatment of cancer offers the attractive possibilities of a novel mechanism of action, thus overcoming drug resistance and increasing the selectivity of drugs for cancerous over healthy cells[60].

It has been shown that lipophilic cationic compounds, such as the complexes synthesised in this work, are attracted to the negatively charged internal transmembrane potential of mitochondria and accumulate within them as a consequence[60]. This potential has been shown to be approximately 60 mV more negative in cancerous cells (CX-1 colon carcinoma cells) than in healthy cells (CV-1 monkey kidney epithelial cells), leading to a 10-fold preference of the compounds for the diseased cells. Once inside the mitochondria, the presence of the lipophilic cations is likely to interfere with cellular ATP production. This disruption to cell viability triggers the apoptotic pathway described above[63].

A number of organic[63] and inorganic compounds have been investigated in this respect, of which the latter comprises mainly gold (I) complexes (e.g. Figure 1.11). These have been shown to induce mitochondrial swelling[58, 60, 64], a precursor event to mitochondrial membrane permeabilisation[59] and apoptosis. The complexes studied in this thesis are also lipophilic and cationic in nature and therefore have the potential to selectively kill cancer cells by a similar mechanism.

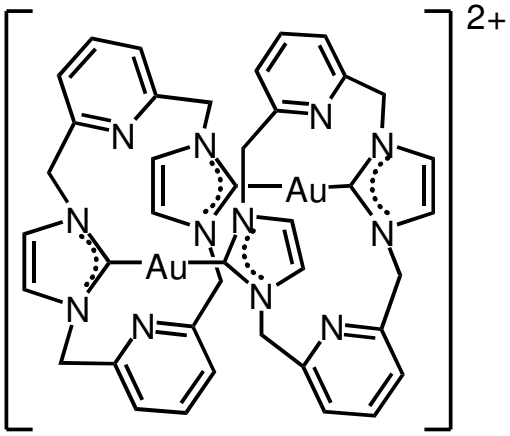

Figure 1.11 The chemical structure of a gold(I) carbene complex. An example of a lipophilic cationic metal complex capable of inducing mitochondrial swelling of carcinoma cells.

1.6.2 DNA Bis-intercalators

Intercalating agents are complexes which are able to insert between layers of base pairs on DNA. This disrupts the shape of the double helix which often results in unwinding of the helix. Such structural modifications can lead to inhibition of replication, transcription and DNA repair[65]. They are therefore attractive for the

treatment of cancer. Intercalators normally consist of at least one planar aromatic unit which is able to form stable hydrophobic stacking interactions with the bases on DNA. There are a number of examples of ruthenium[66] and osmium[67] complexes capable of intercalating into DNA *via* one of its ligands (Figure 1.12). The crystal structure shown in Figure 1.13 illustrates how a similar rhodium complex inserts between the base pairs[68].

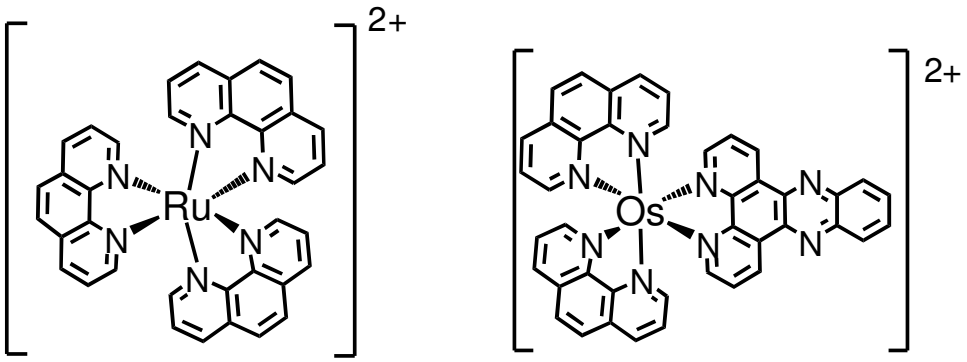

Figure 1.12 The chemical structures of Δ-[Ru(phenanthroline)$_3$]$^{2+}$ [66] (left) and [Os(phenanthroline)$_2$dppz]$^{2+}$ [67] (right). Both these complexes can intercalate into DNA.

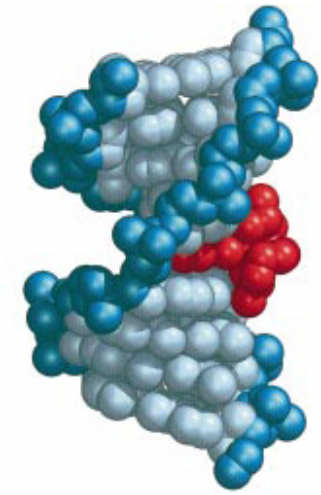

Figure 1.13 Crystal structure of Δ-α-{Rh[(R,R)Me$_2$trien]phi}$^{3+}$ (red) (trien = triethylenetetramine, phi = 9,10-phenanthrenequinone diimine) bound to the oligonucleotide double helix d(GTTGCAAC)$_2$ (blue)[68].

A search of the Cambridge Crystallographic Database reveals that bis-arene complexes of ruthenium and osmium have ligand-ligand distances in the range 3.34 Å to 3.60 Å and 3.51 Å to 3.54 Å, respectively; however it should be noted that there are only two examples of the latter. The base-pair separation for the double-helical, B-form of DNA is 3.36 Å[69]. Since this value falls within the range for ruthenium bis-arene complexes (there are too few osmium examples to assume that they are a true representation of distances) it is theoretically possible to imagine such a complex with two extended aromatic ligands having the potential to act as a bis-intercalator, with both ligands inserting themselves between DNA bases. Using the crystallographic data for a simple ruthenium bis-biphenyl complex[70], a model illustrating this mode of binding to a DNA double helix was created using Sybyl (Ver. 6.3, Tripos Inc.) software and is shown in Figure 1.14. This shows the ruthenium complex docked in the major groove with the two unbound biphenyl rings intercalating between bases. This model was created to illustrate that the relative distances make this type of interaction possible. No attempts were made to perform energy minimisation calculations.

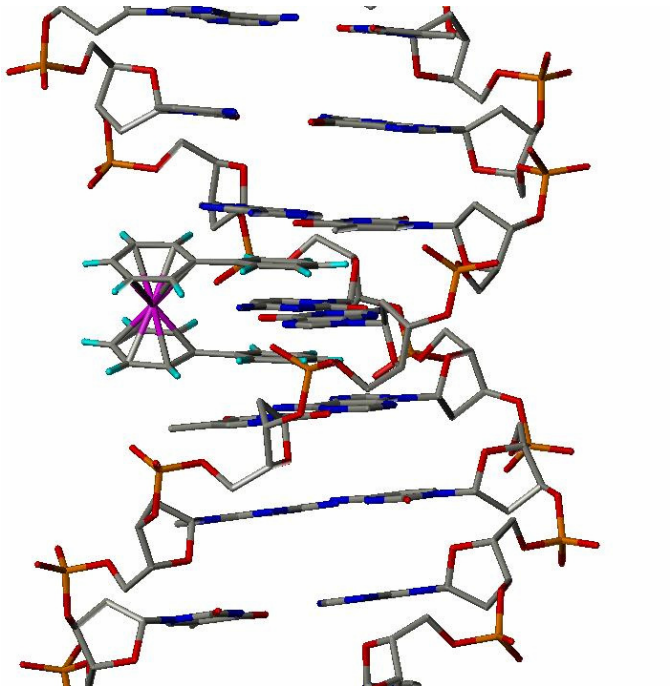

Figure 1.14 Model of how a bis-arene metal complex $[Ru(\eta^6\text{-biphenyl})_2]^{2+}$ [70] might insert itself into the major groove of DNA resulting in bis-intercalation.

To date the only reported examples of metal bis-intercalators involve two metal centres with a carbon linker[71-73]. Binding constants for ruthenium(II) complexes (e.g. Figure 1.15) have been found to be *ca.* 50 orders of magnitude greater than similar mono-intercalating complexes, exemplifying the increase in biological efficacy possible with multiple intercalation sites[73-75]. A similar increase in binding affinity could be envisaged with metal bis-arene structures over similar mono-arene complexes, leading to cytotoxic activity at far lower concentrations.

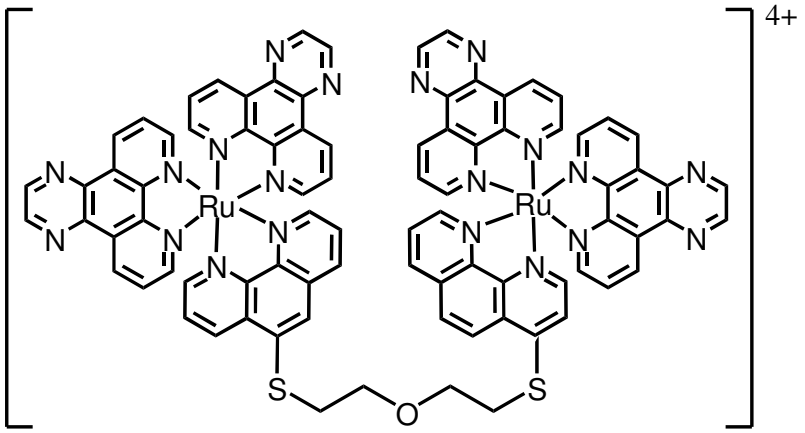

Figure 1.15 The chemical structure of [{Ru(dpq)$_2$(μ-phen-5-S(CH$_2$)$_2$O(CH$_2$)$_2$S-5-phen)]$^{4+}$ (where dpq = dipyrido[3,2-*d*:2',3'-*f*]quinoxaline, phen = 1,10-phenanthroline and SOS = 2-mercaptoethylether), a flexible dinuclear ruthenium complex capable of bis-intercalation into DNA[73].

1.7 Aims

The overall aim of this thesis is to synthesise and investigate the properties of novel unsymmetrical ruthenium(II) and osmium(II) bis-arene complexes incorporating biologically-active ligands. Four groups of ligands are investigated; indole derivatives, aspartame, tamoxifen and flavonoids. Through knowledge gained regarding the chemical and biological properties of the systems, the potential of such an approach to design novel anticancer agents is assessed.

Specific aims of this thesis are as follows.

(1) Synthesise and characterise ruthenium and osmium bis-arene complexes containing a range of biologically-active ligands.

(2) Probe the structure, solution chemistry and stability of the complexes.

(3) Investigate and provide rational explanations for changes to ligand properties on binding to either metal centre.

(4) Investigate the cancer cell cytotoxicity of the complexes and, if active, possible mechanisms of activity.

(5) Draw comparisons between ruthenium and osmium analogues from the results obtained.

1.8 References

[1] L. Ronconi, P. J. Sadler, *Coord. Chem. Rev.,* **2007**, *251*, 1633.

[2] G. Bertrand, *8th Intl Conf. Appl. Chem.,* **1912**, *28*, 30.

[3] P. C. A. Bruijnincx, P. J. Sadler, *Curr. Opin. Chem. Bio.* **2008**, *12*, 197

[4] C. Orvig, M. J. Abrams, *Chem. Rev.* **1999**, *99*, 2201.

[5] S. P. Fricker, *Dalton Trans.,* **2007**, 4903.

[6] Z. Guo, P. J. Sadler, *Adv. Inorg. Chem.,* **2000**, *49*, 183.

[7] www.cancerresearchuk.org.

[8] M. Melchart, P. J. Sadler, *Bioorganometallics, Vol. 1*, Wiley - VCH, Weinheim, **2006**.

[9] Z. Guo, P. J. Sadler, *Angew. Chem., Intl Ed.* **1999,** *38*, 1512.

[10] J. Reedijk, *Proc. Natl Acad. Sci. U.S. A.,* **2003**, *100*, 3611.

[11] J. Reedijk, *Plat. Met. Rev.,***2008**, *52*, 2.

[12] F. S. Mackay, J. A. Woods, H. Mosely, J. Ferguson, A. Dawson, S. Parsons, P. J. Sadler, *Chem. Eur. J.,* **2006**, *12*, 3155.

[13] J. Kasparkova, F. S. Mackay, V. Brabec, P. J. Sadler, *J. Bio. Inorg. Chem.,* **2003**, *8*, 741.

[14] M. J. Clarke, *Coord. Chem. Rev.,***2003**, *236*, 209.

[15] C. S. Allardyce, P. J. Dyson, *Plat. Met. Rev.,* **2001**, *45*, 62.

[16] P. J. Dyson, G. Sava, *Dalton Trans.,* **2006**, 1929.

[17] A. Habtemariam, M. Melchart, R. Fernandez, S. Parsons, I. D. H. Oswald, A. Parkin, F. P. A. Fabbiani, J. E. Davidson, A. Dawson, R. E. Aird, D. I. Jodrell, P. J. Sadler, *J. Med.Chem.,* **2006**, *49*, 6858

[18] R. E. Aird, J. Cummings, A. A. Ritchie, M. Muir, R. E. Morris, H. Chen, P. J. Sadler, *Br. J. Cancer,* **2002,** *86*, 1652.

[19] A. F. A. Peacock, A. Habtemariam, R. Fernandez, V. Walland, F. P. A. Fabbiani, S. Parsons, R. E. Aird, D. I. Jodrell, P. J. Sadler, *J. Am. Chem. Soc.,* **2006**, *128*, 1739.

[20] W.-Y. Sun Raymond, D.-L. Ma, L.-M. Wong Ella, C.-M. Che, *Dalton Trans.,)* **2007**, 4884.

[21] M. J. Clarke, F. Zhu, D. R. Frasca, *Chem. Rev.,* **1999**, *99*, 2511.

[22] T. W. Hambley, *Dalton Trans.,* **2007**, 4929.

[23] Y. K. Yan, M. Melchart, A. Habtemariam, P. J. Sadler, *Chem. Commun.,* **2005**, 4764.

[24] K. Severin, R. Bergs, W. Beck, *Angew. Chem., Intl Ed.,* **1998**, *37*, 1635.

[25] G. Jaouen, A. Vessieres, I. S. Butler, *Acc. Chem. Res.,***1993**, *26*, 361.

[26] U. Schatzschneider, N. Metzler-Nolte, *Angew. Chem., Intl Ed.,* **2006**, *45*, 1504.

[27] P. J. Dyson, W. H. Ange, *PCT Intl Appl.*, **2007**, 39pp.

[28] Griffith, *Comprehensive Coordination Chemistry, Vol. 4*, **1987**.

[29] P. A. Lay, W. D. Harman, *Adv. Inorg. Chem.,***1991**, *37*, 219.

[30] M. L. Tobe, J. Burgess, *Inorganic Reaction Mechanisms*, Addison Wesley Longman Inc., Essex, **1999**.

[31] D. T. Richens, *The Chemistry of Aqua Ions*, Wiley, **1997.**

[32] A. Doadrio, D. Craciunescu, C. Ghirvu, *Anales de la Real Academia de Farmacia* **1980**, *46*, 153.

[33] A. Doadrio, D. Craciunescu, C. Ghirvu, J. C. Nuno, *Anal. Quimica,* **1977,** *73*, 1220.

[34] P. M. Loiseau, D. G. Craciunescu, J. C. Doadrio-Villarejo, G. Certad-Fombona, P. Gayral, *Trop. Med. Parasit.,* **1992**, *43*, 110.

[35] E. A. Seddon, K. R. Seddon, *'The Chemistry of Ruthenium'*, 1st Edition ed., **1984**.

[36] I. Bratsos, S. Jedner, A. Bergamo, G. Sava, T. Gianferrara, E. Zangrando, E. Alessio, *J. Inorg. Biochem.,* **2008**, *102*, 1120

[37] O. Novakova, H. Chen, O. Vrana, A. Rodger, P. J. Sadler, V. Brabec, *Biochemistry* **2003**, *42*, 11544.

[38] R. E. Morris, R. E. Aird, P. d. S. Murdoch, H. Chen, J. Cummings, N. D. Hughes, S. Parsons, A. Parkin, G. Boyd, D. I. Jodrell, P. J. Sadler, *J. Med. Chem.,* **2001**, *44*, 3616.

[39] H. Chen, J. A. Parkinson, S. Parsons, R. A. Coxall, R. O. Gould, P. J. Sadler, *J. Am. Chem. Soc.,* **2002**, *124*, 3064.

[40] Y. Hung, W.-J. Kung, H. Taube, *Inorg. Chem.,* **1981**, *20*, 457.

[41] A. F. A. Peacock, M. Melchart, R. J. Deeth, A. Habtemariam, S. Parsons, P. J. Sadler, *Chem. Eur. J.,***2007**, *13*, 2601.

[42] F. Wang, A. Habtemariam, E. P. L. v. d. Geer, R. Fernandez, M. Melchart, R. J. Deeth, R. Aird, S. Guichard, F. P. A. Fabbiani, P. Lozano-Casal, I. D. H. Oswald, D. I. Jodrell, S. Parsons, P. J. Sadler, *Proc. Natl Acad. Sci. U S A,* **2005**, *102*, 18269

[43] H. Petzold, J. Xu, P. J. Sadler, *Angew. Chem., Int. Ed.,***2008**, *47*, 3008

[44] A. F. A. Peacock, S. Parsons, P. J. Sadler, *J. Am. Chem. Soc.,* **2007**, *129*, 3348.

[45] F. A. Peacock Anna, A. Habtemariam, A. Moggach Stephen, A. Prescimone, S. Parsons, J. Sadler Peter, *Inorg. Chem.,* **2007**, *46*, 4049.

[46] R. Fernandez, M. Melchart, A. Habtemariam, S. Parsons, J. Sadler Peter, *Chem. Eur. J.,* **2004**, *10*, 5173.

[47] S. J. Dougan, A. Habtemariam, S. E. McHale, S. Parsons, P. J. Sadler, *Proc. Natl Acad. Sci. U. S. A., Early Edition* **2008**, 1

[48] S. J. Dougan, M. Melchart, A. Habtemariam, S. Parsons, P. J. Sadler, *Inorg. Chem.,* **2006**, *45*, 10882.

[49] L. H.-K. Liu, F. Wang, J. A. Parkinson, J. Bella, P. J. Sadler, *Chem. Eur. J.,***2006**, *12*, 6151.

[50] M. Melchart, A. Habtemariam, S. Parsons, S. A. Moggach, P. J. Sadler, *Inorg. Chim. Acta,* **2006**, *359*, 3020

[51] R. Castarlenas, M. A. Esteruelas, E. Onate, *Organometallics,* **2005**, *24*, 4343.

[52] K. Matsumura, S. Hashiguchi, T. Ikariya, R. Noyori, *J. Am. Chem. Soc.,* **1997**, *119*, 8738.

[53] A. Schluter, K. Bieber, W. S. Sheldrick, *Inorg. Chim. Acta,* **2002**, *340*, 35.

[54] D. A. Freedman, D. J. Magneson, K. R. Mann, *Inorg. Chem.,* **1995**, *34*, 2617.

[55] J. M. Wolff, W. S. Sheldrick, *J. Organomet. Chem.,***1997**, *531*, 141.

[56] A. Houlton, R. M. G. Roberts, J. Silver, *J. Organomet. Chem.,* **1991**, *418*, 107.

[57] H. Kopf, P. Kopf-Maier, E. W. Neuse, *J. Cancer Res. Clin. Oncol.,* **1984**, *108*, 336.

[58] M. J. McKeage, L. Maharaj, S. J. Berners-Price, *Coord. Chem. Rev.,* **2002**, *232*, 127.

[59] J. Henry-Mowatt, C. Dive, J.-C. Martinou, D. James, *Oncogene,* **2004**, *23*, 2850.

[60] P. J. Barnard, M. V. Baker, S. J. Berners-Price, D. A. Day, *J. Inorg. Biochem.,* **2004**, *98*, 1642.

[61] C. Krieger, M. R. Duchen, *Eur. J. Pharm.* **2002**, *447*, 177.

[62] M. Hirai, S. Suzuki, *Naibunpi, Tonyobyoka,* **2002**, *15*, 374.

[63] J. S. Modica-Napolitano, J. R. Aprille, *Adv. Drug Del. Rev.,***2001**, *49*, 63.

[64] M. P. Rigobello, G. Scutari, R. Boscolo, A. Bindoli, *Br. J. Pharm.,* **2002**, *136*, 1162.

[65] B. M. Zeglis, V. C. Pierre, J. K. Barton, *Chem. Commun.,* **2007**, 4565.

[66] J. G. Collins, A. D. Sleeman, J. R. Aldrich-Wright, I. Greguric, T. W. Hambley, *Inorg. Chem.,***1998**, *37*, 3133.

[67] R. E. Holmlin, J. K. Barton, *Inorg. Chem.,* **1995**, *34*, 7.

[68] K. E. Erkkila, D. T. Odom, J. K. Barton, *Chem. Rev.,* **1999**, *99*, 2777.

[69] F. H. C. Crick, J. D. Watson, *Proc. R. Soc. London, Ser. A,* **1954**, *223*, 80.

[70] K. D. Plitzko, B. Rapko, B. Gollas, G. Wehrle, T. Weakley, D. T. Pierce, W. E. Geiger, Jr., R. C. Haddon, V. Boekelheide, *J. Am. Chem. Soc.,* **1990**, *112*, 6545.

[71] B. Oenfelt, P. Lincoln, B. Norden, *J. Am. Chem. Soc.,* **1999**, *121*, 10846.

[72] J.-Z. Wu, L. Yuan, *J. Inorg. Biochem.,* **2004**, *98*, 41.

[73] C. R. Brodie, J. R. Aldrich-Wright, *Eur. J. Inorg. Chem.,* **2007**, 4781.

[74] F. M. O'Reilly, J. M. Kelly, *New J. Chem.,* **1998**, *22*, 215.

[75] F. O'Reilly, J. Kelly, A. Kirsch-De Mesmaeker, *Chem. Commun.,* **1996**, 1013.

Chapter 2 Experimental Methods

This chapter describes the main experimental techniques used in this work. More specific methods relating to individual experiments are described in the appropriate chapters. The synthesis and characterisation of the starting materials used for synthesis of the ruthenium and osmium complexes in subsequent chapters is also covered here.

2.1 Synthesis of Starting Materials

Ruthenium and osmium dimers of the form $[(\eta^6\text{-arene})MCl_2]_2$ (M = Ru/Os, arene = *p*-cymene/biphenyl) were used as starting materials for the synthesis of the bis-arene complexes studied in this thesis, therefore their preparations are described here. The methods closely follow previously reported procedures[1-3].

2.1.1 Materials

$RuCl_3.xH_2O$ was purchased from Precious Metals Online and $OsCl_3.xH_2O$ from Alfa Aesar (x is assumed to be 3). α–Terpenine was purchased from Sigma-Aldrich. 1,4-Dihydrobiphenyl was prepared by a previously reported procedure[4]. Ethanol was dried by distilling over Mg/I_2 prior to use.

2.1.2 Preparation of Complexes

$[(\eta^6$-*p*-cymene)$RuCl_2]_2$. $RuCl_3.xH_2O$ (4.08 g, 0.02 mol) was dissolved in dry ethanol (120 mL) and following the drop-wise addition of α-terpinene (20 mL, 0.15 mol) the

dark brown solution was heated under reflux at 368 K for 24 h. After cooling, the resulting red solution was filtered to give a deep red powder which was washed with ethanol and diethyl ether and dried overnight *in vacuo*. (Yield: 4.61 g, 75.3%).

Anal. Found %C = 38.89; %H = 4.10. Calc. for $C_{20}H_{28}Cl_4Ru_2$ (M = 612.39): %C = 39.23; %H = 4.61. ^{1}H NMR, 600MHz ($CDCl_3$): δ 1.30 (d, 12H), 2.16 (s, 6H), 2.95 (sp, 2H), 5.35 (d, 4H), 5.50 (d, 4H)

[(η^6-biphenyl)RuCl$_2$]$_2$. $RuCl_3.xH_2O$ (2.05 g, 0.01 mol) was dissolved in dry ethanol (120 mL) and following the addition of 1,4-dihydrophenyl (14.01 g, 0.09 mol) the dark brown solution was heated under reflux at 368 K for 24 h. After cooling, the solution, which had not significantly changed colour, was filtered to give a brown powder which was washed with ethanol and diethyl ether and dried overnight i*n vacuo*. (Yield: 2.80 g, 85.7%).

Anal. Found %C = 43.88; %H = 3.00. Calc. for $C_{24}H_{20}Cl_4Ru_2$ (M = 652.37): %C = 44.19; %H = 3.09. ^{1}H NMR, 600MHz (DMSO-d^6): δ 6.13 (m, 6H), 6.44 (d, 4H), 7.55 (m, 6H), 7.85 (d, 4H).

[(η^6-*p*-cymene)OsCl$_2$]$_2$. $OsCl_3.xH_2O$ (1.06 g, 0.003 mol) was dissolved in dry ethanol (75 mL) and following the drop-wise addition of α-terpinene (5 mL, 0.04 mol) the dark brown solution was heated under reflux at 368 K for 24 h. After cooling, the resulting orange solution was filtered to give a bright orange powder which was washed with ethanol and diethyl ether and dried overnight *in vacuo*. (Yield: 0.78 g, 65.3%).

Anal. Found %C = 30.73; %H = 3.65. Calc. for $C_{20}H_{28}Cl_4Os_2$ (M = 790.71): %C = 30.38; %H = 3.57. ^{1}H NMR, 500MHz ($CDCl_3$): δ 1.32 (d, 12H), 2.21 (s, 6H), 2.80 (sp, 2H), 6.04 (d, 4H), 6.21 (d, 4H)

[(η^6-biphenyl)OsCl$_2$]$_2$. $OsCl_3.xH_2O$ (1.01 g, 0.003 mol) was dissolved in dry ethanol (75 mL) and following the addition of 1,4-dihydrobiphenyl (2.26 g, 0.015 mol) the brown solution was heated under reflux at 368 K for 24 h. After cooling, the resulting orange solution was filtered to give a dark orange powder which was washed with ethanol and diethyl ether and dried overnight *in vacuo*. (Yield: 1.04 g, 88.1%).

Anal. Found %C = 35.25; %H = 2.11. Calc. for $C_{24}H_{20}Cl_4Os_2$ (M = 830.69): %C = 34.70; %H = 2.43. ^{1}H NMR, 600MHz (DMSO-d_6): δ 6.30 (t, 4H), 6.36 (t, 2H), 6.64 (d, 4H), 7.45 (m, 6H), 7.71 (d, 4H).

2.2 Nuclear Magnetic Resonance Spectroscopy[5-7]

Nuclear magnetic resonance (NMR) spectroscopy is a powerful tool which can be used to probe the structure and properties of both organic and inorganic species. The main nucleus studied in this thesis is ^{1}H, although a few two-dimensional experiments were carried out using ^{13}C. ^{1}H NMR spectroscopy was utilised to characterise and explore the solution chemistry of the complexes synthesised.

2.2.1 Overview of Technique

NMR spectroscopy involves the study of induced transitions between nuclear spin energy levels, whose degeneracy has been removed by the presence of a magnetic field. The magnetic moment (μ), which is characteristic of a specific nucleus, is defined by the equation:

$$\mu = \gamma \hbar I$$

where γ is the gyromagnetic ratio, ħ is h/2π (h = Planck's constant) and I is the spin quantum number. It has no directional preference, however in the presence of a magnetic field (B_o, Tesla) its orientation becomes quantised and dependent on I through the equation:

$$\mu_z = \gamma \hbar m_I$$

where m_I is the magnetic quantum number, which has 2I + 1 integral values between +I and –I.

To illustrate this, Figure 2.1 shows the two quantised levels of the nuclear magnetic moment for a nucleus with I = ½. These move in circular paths (precession) around the z-axis with the Larmor Frequency (ν_o), defined by $\nu_o = \gamma B_o/2\pi$. There is a preference for alignment of spins along the direction of B_o (+z) rather than against it (-z) and the population difference between these states is given by Boltzmann's Law: $n(+½)/n(-½) = \exp(\Delta E/kT)$ where n is the population of the spin state and k is Boltzmann's constant.

In NMR experiments, the application of a second field, B_1, at the Larmor frequency, causes these two states to interconvert with absorption of energy occurring on the +z

to –z transition and emission on the –z to +z transition. Due to the excess of +z spins, there is a net absorption of energy, known as *resonance*, which can be plotted versus frequency. Modern techniques use pulsed experiments, in which the nuclei are briefly irradiated periodically with an intense B_1 field (length ~ < 10 μs). Between these pulses the spins relax to their original states leading to a decrease in magnetisation, known as the free induction decay (FID). This FID is Fourier transformed to give the experimental spectrum with signals as a function of frequency.

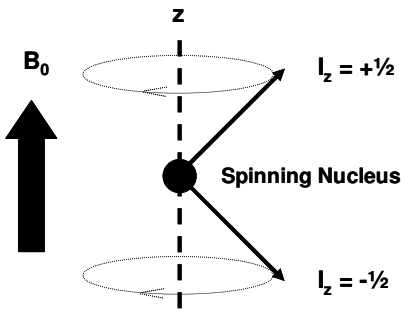

Figure 2.1 The alignment of nuclear magnetic moments in the presence of the magnetic field, B_o, for a nucleus with I = ½.

The observed resonance frequency (ν_o) is not only dependent on γ and B_o, but also on the molecular environment of the nucleus as a result of the electron cloud surrounding it also possessing a magnetic moment. This phenomenon is known as (de)shielding and the variation in frequency as a result is termed the *chemical shift*. Furthermore, if another nucleus is nearby which also has a spin, the magnetic environment is also affected by this resulting in the appearance of a multiplet rather than a singlet. This *spin-spin coupling* is measured by the coupling constant, *J* (Hz),

and the nature of the multiplicities follows the 2nI + 1 rule, illustrating that it depends both on the nature and number of nearby spins.

2.2.2 Water Supression

A large majority of the NMR experiments performed in this thesis were on samples in aqueous solution (100% D_2O or 95% H_2O/5% D_2O) so as to be of biological relevance. However, the use of such solvents results in a large HOD signal in the spectrum which requires suppression. This was achieved by either pre-saturation or Shaka[8] techniques. Pre-saturation involves saturating the water peak by irradiating with the frequency of the water signal in between pulse sequences. Shaka water suppression, or Double Pulse Field Gradient Spin Echo (DPFGSE), uses pulsed field gradient spin echos in which the refocusing pulse is the sequence soft $\pi(x)$-hard $\pi(-x)$[8]. A disadvantage of the latter technique is that signals which resonate close to the water peak are also suppressed and therefore reduced in intensity.

2.2.3 Two-Dimensional Techniques

2.2.3.1 COrrelation and TOtal Correlation Spectroscopy (COSY and TOCSY)

Correlation spectroscopy (COSY) is a two-dimensional homonuclear (^1H-^1H) technique which allows geminally (two-bond) or vicinally (three-bond) coupled protons to be identified by off-diagonal cross-peaks as a result of magnetisation

transfer between nuclei. Total correlation spectroscopy (TOCSY) is a similar technique to COSY, however coupling between all protons in the same spin system may be now observed through cross-peaks. This long-range correlation is obtained by maximizing the transfer of magnetisation by extending the length of the time delay between pulses, known as the mixing time. The latter technique is particularly useful in assigning spectra which correspond to a mixture of compounds.

2.2.3.2 Nuclear Overhauser Effect Spectroscopy (NOESY)

Nuclear Overhauser Effect spectroscopy (NOESY) is also a two-dimensional homonuclear (^{1}H-^{1}H) technique. It relies on the transfer of magnetisation from one proton to another through dipolar interactions on irradiation at the frequency of one of the nuclei. This phenomenon is known as the Nuclear Overhauser Effect. Similar to the TOCSY technique described previously, the mixing time is very important and should be as long as possible to allow for the maximum correlation between protons to be achieved. NOESY is a valuable technique for distinguishing between structures with clear stereochemical differences.

2.2.3.3 Heteronuclear Spin-Quantum Coupling Spectroscopy (HSQC)

Heteronuclear Spin-Quantum Coupling Spectroscopy (HSQC) facilitates couplings between protons and other nuclei (^{15}N, ^{31}P, ^{29}Si, ^{13}C for example) to be observed as cross-peaks on a two-dimensional spectrum. The experiments carried out in this thesis only involved proton-carbon (^{1}H-^{13}C) correlation and the magnetisation transfer between these nuclei allowed for the identification of protons bonded to

specific carbon atoms, therefore assisting with complete assignment of ^{1}H and ^{13}C resonances. Quaternary carbons are invisible to the technique since they possess no C-H bonds.

2.2.4 Experimental

All NMR spectra were recorded in 5 mm quartz NMR tubes at 298 K (unless otherwise stated) on either a Bruker DMX 500 (^{1}H = 500.13 MHz) or AVA 600 (^{1}H = 599.81 MHz) spectrometer using TXI [^{1}H, ^{13}C, ^{15}N] or TBI [^{1}H, ^{13}C, ^{15}N] probe-heads equipped with z-field gradients. 1D and 2D spectra were recorded using standard pulse sequences modified by Mr Juraj Bella or Dr Dusan Uhrin, University of Edinburgh. ^{1}H NMR chemical shifts were internally referenced to 1,4-dioxane (3.75 ppm) for aqueous solutions containing D_2O, C*H*Cl_3 (7.27 ppm) for chloroform-*d*$_1$, (C*H*D_2)(CD_3)SO (2.52 ppm) for DMSO-*d*$_6$ and MeO*H* (3.32 ppm) for methanol-*d*$_4$. All data processing was carried out using XWIN-NMR, Bruker UK Ltd (Version 2.0 or 3.6).

2.3 pH Measurements

pH values were measured at *ca.* 298 K using a Coring 240 pH meter equipped with a Therom microcombination KCl (chloride) / KNO_3 (chloride free) electrode calibrated with Aldrich standard buffer solutions at pH 4, 7 and 10. pH* values (pH meter readings without correction for effects of D on glass electrode) of NMR samples in D_2O were measured directly in the NMR tube by the same method.

2.4 Calculation of pK_a Values

pK_a values (the negative logarithm of the acid dissociation constant, K_a) were calculated through the use of NMR spectroscopy by the following method.

The pH* values of solutions of the complexes in D_2O were measured at *ca.* 298 K directly in the NMR tube before and after recording NMR data to obtain an average pH* value. The pH* values were varied from *ca.* 2 to *ca.* 11 by the addition of dilute NaOD or $DClO_4$. ^1H NMR spectra were recorded and chemical shifts plotted against pH*. The resultant pH* titration curves were fitted to the Henderson-Hasselbalch equation using the program ORIGIN 7.5[9].

For the (de)protonation: $HA \rightleftharpoons H^+ + A^-$

The Henderson-Hasselbalch Equation: $pH = pK_a + \log_{10}([A^-]/[HA])$

So that when half-dissociated: $[HA] = [A^-]$ and $pH = pK_a$

As a result of the fast exchange processes on the NMR timescale, the observed chemical shifts can be considered as weighted averages according to the populations of the protonated and deprotonated species. The modified Henderson-Hasselbalch equation is shown below, where δ_{obs} is the chemical shift at a given pH and δ_{HA} and δ_{A^-} are the chemical shifts at low and high pH respectively[10, 11].

$$\delta_{obs} = \frac{\delta_{HA} + \delta_{A^-} \times 10^{(pKa^* - pH^*)}}{1 + 10^{(pKa^* - pH^*)}}$$

The errors in the pK_a* values obtained are estimated to be ± 0.05 pK units. The pK_a* values were converted to pK_a values by the use of the equation pK_a = 0.929pK_a* + 0.42, suggested by Krezel and Bal[12], for comparison with related values in the literature.

2.5 Electrospray Ionisation Mass Spectrometry

Electrospray ionisation mass spectra (ESI-MS) were obtained on a Micromass Platform II Mass Spectrometer or a Micromass ZMD Mass Spectrometer (Micromass, Manchester UK) and solutions were infused directly at a rate of 5-30 µL/min. The capillary voltage was 3.5 kV and the cone voltage was varied between 10 and 40 V depending on sensitivity. The source temperature and mass range scanned were varied depending on the nature of the solution under investigation. Data acquisition was obtained on a MassLynx (Version 2.5) Windows NT PC data system.

2.6 Ultraviolet-visible Spectroscopy

Ultraviolet-visible (UV/Vis) spectroscopy was carried out on a Perkin-Elmer Lambda-16 UV/Vis spectrophotometer using 1 cm path-length quartz cuvettes and a PTP1 Peltier Temperature Controller. Unless otherwise stated, spectra were recorded at 298 K over a range of 800 – 200 nm at a scan rate of 420 nm min^{-1} and were processed using UV-Winlab software for Windows 95.

2.7 Electrochemistry

Electrochemistry was carried out using platinum microworking and counter electrodes and an Ag/AgCl reference electrode. Analysis of experimental data was carried out using General Purpose Electrochemical System (GPES), version 4.8 software, connected to an Autolab PGSTAT10 potentiostat. The inert electrolyte was tetrabutylammonium tetrafluoroborate ($TBABF_4$) and solutions contained 0.1 M $TBABF_4$ in *N,N*-dimethylformamide (DMF). All potentials were referenced to the ferrocene/ferrocinium couple (+0.55 V vs. standard calomel electrode, SCE) and coherency ensured by cleaning the working electrode with emery paper between measurements. Solutions were purged with dry nitrogen prior to study.

2.8 X-ray Crystallography

All diffraction data were collected and refined by Professor Simon Parsons and colleagues at The University of Edinburgh on a Bruker (Siemens) Smart Apex CCD Diffractometer using $Mo_{K\alpha}$ radiation equipped with an Oxford Cryosystems low-temperature device operating at 150 K. Structures were solved using direct (SHELXL-97[13]) methods and were refined against F^2 using CRYSTALS[14]. H atoms were placed in calculated positions and non-H atoms were modelled with anisotropic displacement parameters. The modelling programs Mercury 1.4 and Diamond 3.0 were used for analysis of data and generation of graphics.

2.9 Circular Dichroism

Circular dichroism (CD) data was obtained using a Jasco J-810 CD Spectropolarimeter with 1 mm path-length quartz cuvettes (300 – 400 μL) and a Peltier temperature control unit. A constant flow of high purity nitrogen was supplied from a nitrogen generator. Spectra were recorded at 310 K from 500-200 nm unless otherwise stated and were processed using Jasco Spectra Manager software.

2.10 High Performance Liquid Chromatography

High Performance Liquid Chromatography (HPLC) was performed on a Gilson HPLC system with a NC100-5C18 reversed-phase column (250 × 4.6 mm, 100 Å, 5 μm, Hicrom). The mobile phases were A: water (purified using a Millipore Elix 5 system) containing 0.1% trifluoroacetic acid (TFA) and B: acetonitrile (for HPLC application, Fischer Chemicals) containing 0.1% TFA with a flow rate of 1.0 mL min^{-1}. The gradients used were dependent on the analysis mixture. Data were collected and analysed by Gilson applications Unipoint software (Version 3.0).

2.11 Elemental Analysis

Carbon, hydrogen and nitrogen (CHN) elemental analysis were carried out at either The University of Edinburgh in the School of Chemistry on an Exeter Analytical Elemental Analyser (CE440), or at The University of St. Andrews in the School of Chemistry on a Carlo Erba CHNS Analyser

2.12 Cytotoxicity Testing

Cytotoxicity assays were performed on human ovarian A2780 and human lung A549 cancer cell lines by Mr Daniel Cole and colleagues at Oncosense Ltd, MMI group, Cambridge, UK. As a measure of cytotoxicity, the concentration of the complex added to the cells which causes 50% inhibition of cell growth, termed the IC_{50} value, is determined. The cells were exposed to a number of different concentrations of the complexes typically ranging from 0.1 to 100 μM for 24 hours. Each concentration was tested in triplicate and two controls were used; a blank with no drug present and cisplatin, to act as a comparison. After 24 hours, the complexes were removed and the cells allowed to recover for 96 hours. The percentage cell survival was then determined using the Sulforrhodamine-B (SRB) assay[15] assuming 100% cell survival for the blank control. Percentage cell survival was then plotted versus complex concentration and the data fitted to the best-fit sigmoidal curve to obtain the IC_{50} value for each complex. A typical example of such a plot is shown in Figure 2.2.

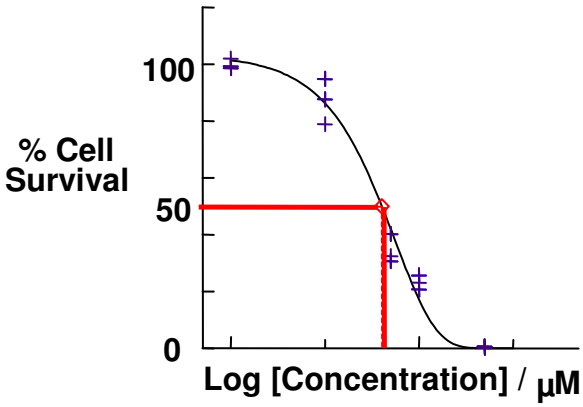

Figure 2.2 A typical plot of percentage cell survival versus concentration obtained from cytotoxicity testing. The IC_{50} value for a complex can be determined by reading off the concentration which leads to 50% cell survival (red line).

2.13 References

[1] A. F. A. Peacock, A. Habtemariam, R. Fernandez, V. Walland, F. P. A. Fabbiani, S. Parsons, R. E. Aird, D. I. Jodrell, P. J. Sadler, *J. Am. Chem. Soc.,* **2006**, *128*, 1739.

[2] R. E. Morris, R. E. Aird, P. d. S. Murdoch, H. Chen, J. Cummings, N. D. Hughes, S. Parsons, A. Parkin, G. Boyd, D. I. Jodrell, P. J. Sadler, *J. Med. Chem.,* **2001**, *44*, 3616.

[3] R. Fernandez, M. Melchart, A. Habtemariam, S. Parsons, P. J. Sadler, *Chem. Eur. J.,* **2004**, *10*, 5173.

[4] D. F. Lindow, C. N. Cortez, R. G. Harvey, *J. Am. Chem. Soc.,* **1972**, *94*, 5406.

[5] P. J. Hore, *Nuclear Magnetic Resonance*, Oxford University Press, New York, **1995**.

[6] A. E. Derome, *Modern NMR Techniques for Chemistry Research*, Pergamon Press, Oxford, **1987**.

[7] J. B. Lambert, H. F. Shurvell, D. A. Lightner, R. G. Cooks, *Organic Structural Spectroscopy*, Prentice-Hall, Upper Saddler River, New Jersey, **1998**.

[8] T.-L. Hwang, A. J. Shaka, *J. Mag. Res., Series A* **1995**, *112*, 275.

[9] Origin, 7.5 Ed., OriginLab Corporation, Northampton, **2006**.

[10] R. Tribolet, H. Sigel, *Eur. J. Biochem.,* **1987**, *163*, 353.

[11] S. A. Lee, R. Eyeson, M. L. Cheever, J. Geng, V. V. Verkhusha, C. Burd, M. Overduin, T. G. Kutateladze, *Proc. Natl. Acad. Sci. U. S. A.,* **2005**, *102*, 13052.

[12] A. Krezel, W. Bal, *J. Inorg. Biochem.,* **2004**, *98*, 161.

[13] G. M. Sheldrick, *SHELXL-97: Program for the refinement of crystal structures*, University of Gottingen, Federal Republic of Germany, **1997**.

[14] P. W. Betteridge, J. R. Carruthers, R. I. Cooper, K. Prout, D. J. Watkin, *J. Appl. Crystallogr.,* **2003**, *36*, 1487.

[15] P. Skehan, R. Storeng, D. Scudiero, A. Monks, J. McMahon, D. Vistica, J. T. Warren, H. Bokesch, S. Kenney, M. R. Boyd, *J. Natl Cancer Inst.,* **1990**, *82*, 1107.

Chapter 3 Ruthenium Complexes of Indole Derivatives

3.1 Introduction

Amino acids and peptides form an important group of biologically-active ligands and sometimes provide simple models for metal adducts with proteins. In addition they offer the possibility of probing the stereo-electronic requirements of specific receptor sites. Metal binding to amino acids in the active site is a key process for the function of a number of enzymes[1]. In an attempt to better understand the interactions observed, a number of metal-amino acid isolated systems have been studied in recent years. Previous work has focussed predominantly on metal binding via carboxylate, amino[2] and sulphur groups[3, 4] however, more recently, a number of full and half-sandwich complexes have been prepared with η^6-coordination to an aromatic side-chain[5]. A range of organometallic derivatives of phenylalanine, tryptophan and tyrosine have been synthesised for metals such as ruthenium, iron, manganese and chromium through η^6-coordination[2, 5, 6]. This Chapter discusses the synthesis, characterisation and properties of ruthenium complexes of two derivatives of indole which are very closely related to the amino acid L-tryptophan (Figure 3.1).

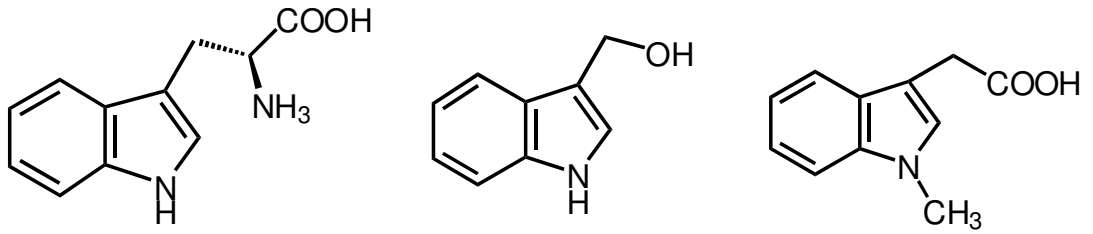

L-tryptophan Indole-3-carbinol 1-methylindole-3-acetic acid

Figure 3.1: The chemical structures of L-tryptophan and the two indole derivatives studied in this work.

Indole-3-carbinol is a naturally-occurring component of *Brassica* vegetables (e.g. cabbage, broccoli, cauliflower), formed during the enzymatic hydrolysis of indole glucosinolates on the cooking or chewing of such foodstuffs, and has shown potential as a chemopreventitive agent[7]. It is known to suppress cell proliferation and induce apoptosis in a number of cancers including prostate, ovarian and colon and has entered phase I and II clinical trials for the prevention of breast cancer[8]. A number of mechanisms for its activity have been proposed, however it is now widely accepted that indole-3-carbinol is a pro-drug which, on digestion, is converted by acid condensation and oligomerisation to a number of active metabolites[9]. The anticancer effects observed are thought to be due to the ability of these metabolites to interfere with the production of a number of key enzymes, including Akt protein kinase[8] and cytochrome P450[9].

Indole-3-acetic acid (auxin) is a plant growth hormone and is also found in mammals through consumption of vegetables and the metabolism of tryptophan[10]. Along with a number of its derivatives (including 1-methylindole-3-acetic acid), it induces apoptosis in mammalian cells (including tumour cells) through generation of radicals and reactive oxygen species as a result of oxidation by certain peroxidases[11-13]. Significantly, mammalian peroxidase does not exert this effect and therefore selective targeting of indole-3-acetic acid and an active enzyme (e.g. horseradish peroxidase) to a tumour is a promising strategy to significantly reduce side-effects and healthy tissue damage[14]. Its application in photodynamic therapy has also been identified; when used in conjunction with a photosensitising dye it has the potential to enhance the treatment of hypoxic tumours by generating reactive oxygen species without the need for high oxygen concentrations[15]. Various metal complexes of

indole-3-acetic acid and its derivatives have been synthesised, a number of which possess interesting biological activity[16, 17].

It is of interest to study organometallic complexes of these ligands as the latter's bioactivity may be enhanced as a result of combination with the properties inherent to the metal. This has the potential to lead to drugs with wider spectra of activity and novel mechanisms of action. In addition, it is also possible that the metal could act as a carrier for the ligand, facilitating novel movement around the body and allowing delivery of the ligand to different targets. Confidence of the ability of the indole derivatives studied in this Chapter to form complexes with ruthenium came from the fact that the binding of L-tryptophan and its derivatives to ruthenium via η^6-coordination is described in the literature,[5, 18] and bis-arene complexes of indole and indoline have also been successfully synthesised[19, 20].

3.2 Experimental

3.2.1 Materials

The starting material $[(\eta^6\text{-}p\text{-cymene})RuCl_2]_2$ was prepared as described in Chapter 2. Indole-3-carbinol, 1-methyl-indole-3-acetic acid, silver trifluoromethanesulfonate (AgOTf) and silver hexafluorophosphate ($AgPF_6$) ($\geq$ 99%) were purchased from Sigma-Aldrich. Acetone was dried prior to use by refluxing with K_2CO_3.

3.2.2 Synthesis

[(η^6-*p*-cymene)Ru(η^6-indole-3-carbinol)](OTf)$_2$ (1) [(η^6-*p*-cymene)RuCl$_2$]$_2$ (0.03 g, 0.05 mmol) was stirred in dry acetone (5 mL) with AgOTf (0.05 g, 0.20 mmol) for 30 min at ambient temperature. The mixture was subjected to gravity filtration of the AgCl precipitate followed by centrifugation to give a clear red solution. Solvent removal under vacuum afforded a red, oily solid of the intermediate [(η^6-*p*-cymene)Ru(acetone)$_3$](OTf)$_2$. This was re-dissolved in dry acetone (5 mL) and indole-3-carbinol (0.015 g, 0.10 mmol) added to the solution. The flask was wrapped in aluminium foil and the translucent red, solution was stirred for 18 h at 298 K. Addition of diethyl ether to the solution afforded a sticky red residue which could not be filtered. Therefore, the solvent was removed under vacuum and the product dried *in vacuo*.

Anal. ^{1}H NMR, 500MHz (*d*$_6$-DMSO): δ 1.23 (dd, 6H, cymene), 2.11 (s, 3H, cymene), 2.80 (sp, 1H, cymene), 3.91 (d, 1H, indole CH$_2$), 4.69 (d, 1H, indole CH$_2$), 5.94 (d, 1H, indole Ph), 6.07 (d, 1H, indole Ph), 6.11 (m, 1H, indole Ph), 6.40 (d, 2H, cymene), 6.51 (d, 2H, cymene), 6.93 (m, 1H, indole Ph), 7.19 (d, 1H, indole CH), 7.99 (s, 1H, indole NH).

A number of synthetic methods were explored for this complex, with the above route giving the best results, however the hygroscopic nature and fast rate of decomposition of this product did not allow for full characterisation. Details of the other synthetic methods attempted are be discussed in Section 3.3 and 3.4.

[(η^6-*p*-cymene)Ru(η^6-1-methylindole-3-acetic acid)](PF_6)$_2$ (2) [(η^6-*p*-cymene)$RuCl_2$]$_2$ (0.10 g, 0.16 mmol) was stirred in dry acetone (6 mL) with $AgPF_6$ (0.16 g, 0.64 mmol) for 30 min at ambient temperature. Filtration of the AgCl precipitate was carried out under Schlenk conditions yielding a transparent red solution. Excess solvent was removed under vacuum, affording a red oily residue of the intermediate [(η^6-*p*-cymene)Ru(acetone)$_3$](PF_6)$_2$. A solution of 1-methylindole-3-acetic acid (0.061 g, 0.32 mmol) in trifluoroacetic acid (TFA) (6 mL) was added to the Schlenk flask and the clear red solution stirred for 20 h at 333 K. After cooling, addition of diethyl ether to the resulting cloudy orange solution yielded a yellow powder which was filtered under gravity and dried *in vacuo* (Yield: 82 mg, 36.2%). Long yellow needle crystals of **2** suitable for X-ray diffraction were obtained by slow diffusion of gaseous diethyl ether into a methanol solution of the complex at 298 K.

Anal. Found %C = 34.85; %H = 2.95; %N = 1.71. Calc. for $C_{21}H_{25}NO_2RuP_2F_{12}$ (M = 714.43): %C =35.29; %H =3.53; %N =1.96. ESI MS: Calc. for $C_{21}H_{24}NO_2Ru$ [M-H-2PF_6]$^+$ *m/z* 424.04, found 424.15. ^{1}H NMR, 500MHz (D_2O): δ 1.24 (dd, 6H, cymene), 1.93 (s, 3H, cymene), 2.71 (sp, 1H, cymene), 3.39 (s, 3H, indole N-CH_3), 3.45 (s, 2H, indole aliphatic CH_2), 6.41 (d, 1H, cymene), 6.55 (t, 1H, Ph), 6.60 (m, 3H, cymene + Ph), 6.74 (d, 1H, cymene), 7.64 (d, 1H, Ph), 7.70 (d, 1H, Ph), 8.25 (s, 1H, indole).

3.2.3 Methods

3.2.3.1 X-ray Crystallography

Diffraction data for **2** were collected and refined as described in Chapter 2. The modelling programs Mercury 1.4 and Diamond 3.0 were used for analysis of data and generation of graphics.

3.2.3.2 Calculation of pK_a Values

For determination of the pK_a values for **2**, the pH* (pH values for D_2O solutions) of the complex in D_2O, containing 1% dioxane as an internal reference, was varied from *ca.* pH* 1.8 to *ca.* 8.5 by the addition of dilute NaOD and ^{1}H NMR spectra recorded. The pK_a values were obtained from the resultant data as described in Chapter 2.

3.2.3.3 Stability Studies

A solution of **2** in 95% H_2O / 5% D_2O at pH 7.04 (10 mM phosphate buffer) was prepared and ^{1}H NMR spectra recorded at 310 K at time intervals of 3 h for 48 h followed by a final measurement after 72 h. The percentage of intact bis-arene complex present in solution at a particular time period was determined by peak-integration relative to the internal reference (1% dioxane). The rate of decomposition of the complex was obtained by plotting these percentages versus time and fitting the data to the appropriate equation for first-order kinetics using the program ORIGIN 7.5[21].

3.2.3.4 High Performance Liquid Chromatography – Electrospray Ionisation Mass Spectrometry (HPLC-ESI-MS)

A Waters 2690 HPLC system using a NC100-5C18 reversed-phase column (250 × 4.6 mm, 100 Å, 5 μm, Hicrom) was interfaced with a Platform II mass spectrometer (Micromass, Manchester, U.K.) for the detection of positive ions. The mobile phase was A: water (purified using a Millipore Elix 5 system) containing 0.1% TFA and B: acetonitrile (for HPLC application, Fischer Chemicals) containing 0.1% TFA with a flow rate of 1.0 mL min^{-1}. The gradient used was 90% A / 10% B for the first 5 minutes then increase B to 90% over 20 minutes. The spray voltage and the cone voltage were 3.50 kV and 20 V respectively. The capillary temperature was 413 K with a 450 L h^{-1} flow of nitrogen drying gas. The quadrupole analyser operated at a background pressure of 2×10^{-5} Torr and scanned at a rate of 900 Da s^{-1}. Data were collected and analysed on a Mass Lynx (version 3.5) Windows NT PC data system using the Max Ent Electrospray software algorithm and calibrated versus an NaI calibration file.

3.2.3.5 Cytotoxicity Testing

Cytotoxicity assays for **2** were performed against human ovarian A2780 and human lung A549 cancer cell lines by Mr Daniel Cole and colleagues at Oncosense Ltd, MMI group, Cambridge, UK as described in Chapter 2.

3.3 Results

Due to the vast differences in properties between the two complexes investigated in this Chapter, experiments on them will be described separately.

3.3.1 [(η^6-*p*-cymene)Ru(η^6-indole-3-carbinol)](OTf)$_2$ (1)

As pointed out in Section 3.2, in order to synthesise [(η^6-*p*-cymene)Ru(η^6-indole-3-carbinol)](OTf)$_2$ a number of approaches were attempted. A range of solvents were explored including acetone, dichloromethane and trifluoroacetic acid. Reaction temperatures and times were also varied from 298 K to 353 K and from 1 h up to 48 h, respectively. In each case, the product was very hygroscopic and appeared to decompose on contact with air with a distinct colour change from dark orange to black, or in some cases deep purple, making full characterisation impossible. On analysis of these products by ^{1}H NMR, the signals obtained were of very poor quality and all showed a broad signal in the aromatic region between 7 and 8 ppm. This was indicative of decomposition of the desired product into a number of species and also suggested polymer formation. The latter point was further implied by the high melting points of the products (573 – 598 K) and their low solubility. Attempts to purify the products of each reaction by a variety of methods resulted in no improvement to the ^{1}H NMR spectra.

The best results were obtained with the method outlined in Section 3.2.2 using dry acetone at 298 K for 18 h, however the product remained highly hygroscopic, preventing full analysis. The aromatic region of the ^{1}H NMR spectrum is shown in

Figure 3.2 (A). η^6-Coordination to ruthenium is confirmed by the characteristic upfield shift[6, 19] of the majority of signals corresponding to indole-3-carbinol compared to the free ligand, in addition to the slight downfield shift of the *p*-cymene protons relative to the half-sandwich starting material[5]. However, it appears that there is some unreacted mono-arene starting material present due to the presence of the doublet of doublets at 5.8 ppm which most likely corresponds to the *p*-cymene aromatic protons (**x**, Figure 3.2). The observation of the broad peak centred at 7 ppm could also suggest that some degree of oligomerisation has taken place. Attempts to separate components of this mixture by both column and high performance liquid chromatography were unsuccessful. Furthermore, re-recording of the spectrum after 3 h resulted in dramatic changes as can be seen in Figure 3.2 (B). All structure to the signals has been lost with only a very broad band present in the aromatic region. This strongly suggests that [(η^6-*p*-cymene)Ru(η^6-indole-3-carbinol)](OTf)$_2$ rapidly degrades in solution.

The lack of stable complex formation combined with the inability to isolate and manipulate the desired product rendered [(η^6-*p*-cymene)Ru(η^6-indole-3-carbinol)](OTf)$_2$ **(1)** unsuitable for further study and therefore lead to the termination of work with this ligand.

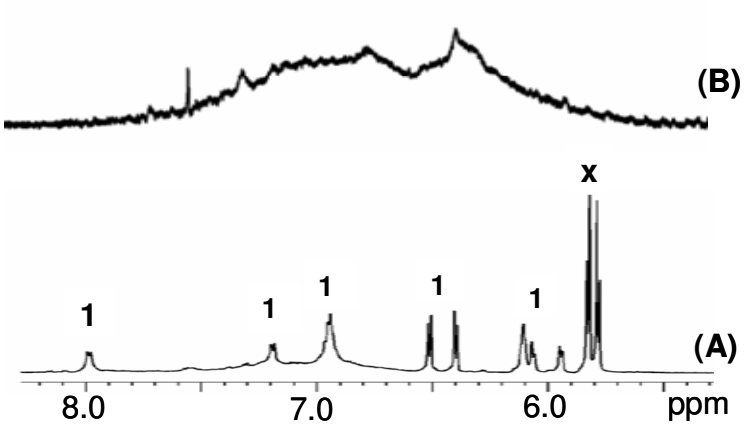

Figure 3.2 Aromatic region of ^{1}H NMR spectrum (d_6-DMSO, 500 MHz) of **1** after (A) 0 h and (B) 3 h in solution. Signals corresponding to **1** and a mono-arene impurity (**x**) are labelled.

3.3.2 [(η^6-*p*-cymene)Ru(η^6 - 1 – methylindole – 3 - acetic acid)](PF_6)$_2$ (2)

3.3.2.1 Synthesis and Structure

The ruthenium(II) bis-arene complex [(η^6-*p*-cymene)Ru(η^6 - 1 – methylindole – 3 - acetic acid)](PF_6)$_2$ (**2**) was successfully synthesised in a good yield from the corresponding chloro-bridged dimer [(η^6-*p*-cymene)$RuCl_2$]$_2$ and was characterised using ^{1}H NMR spectroscopy, ESI-MS and elemental analysis. The data obtained are consistent with the sandwich structure shown in Figure 3.3

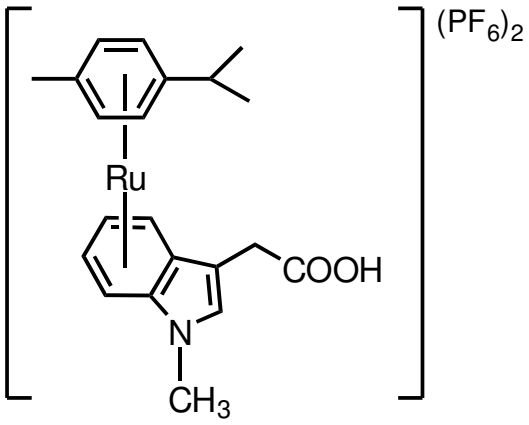

Figure 3.3 Chemical structure of [(η^6-*p*-cymene)Ru(η^6-1-methylindole-3-acetic acid)]$(PF_6)_2$ (**2**).

3.3.2.2 X-ray Crystallography

The X-ray crystal structure of [(η^6-*p*-cymene)Ru(η^6-1-methylindole-3-acetic acid)]$(PF_6)_2$ (**2**) was obtained and is shown in Figure 3.4. It can be seen that the complex has crystallised as the methyl ester (**2a**), most likely due to the use of methanol in the crystallisation process. The structure shows the predicted bis-arene 'sandwich' geometry with all six carbon atoms from both ligands involved in π–bonding to the ruthenium. Both bound phenyl rings appear to have regular geometries, with no significant angle distortions and have a staggered conformation with respect to each other. The ruthenium atom is not positioned centrally between the two arenes, but is closer to the *p*-cymene ligand with Ru-cymene$_{(centroid)}$ = 1.707 Å and Ru-indole$_{(centroid)}$ = 1.757 Å. This suggests that the *p*-cymene possesses a greater interaction and better orbital overlap with the metal than 1-methylindole-3-acetic acid. Crystallographic data are shown in Table 3.1 and selected bond lengths

and angles are listed in Table 3.2. The numbering scheme corresponds to that in Figure 3.4.

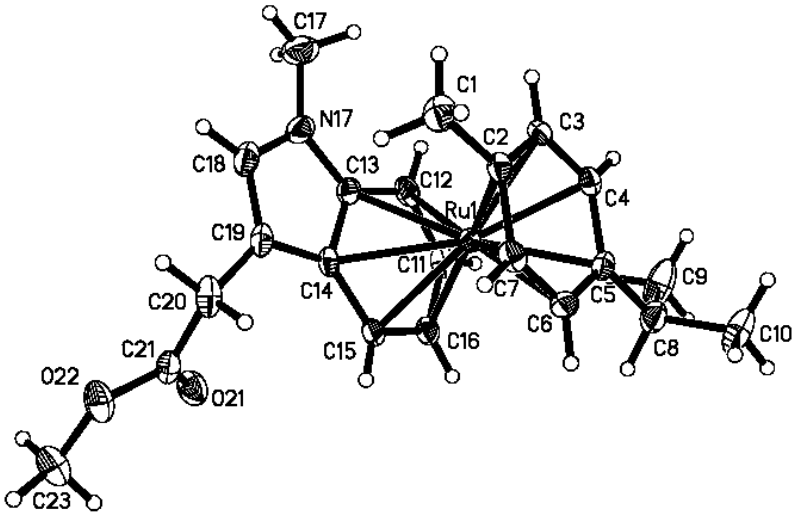

Figure 3.4 X-ray crystal structure and atom numbering scheme for [(η^6-*p*-cymene)Ru(η^6-1-methyl-3-indolemethyl acetate)]$(PF_6)_2$ **(2a).** Thermal ellipsoids at 50% probability level.

Table 3.1 Crystallographic data and solution refinements for [(η^6-*p*-cymene)Ru(η^6-1-methyl-3-indolemethyl acetate)]$(PF_6)_2$ (**2a**).

	[(η^6-*p*-cymene)Ru(η^6-1-methyl-3-indolemethyl acetate)]$(PF_6)_2$ (2a)
Formula	$C_{22}\ H_{27}\ F_{12}\ N\ O_2\ P_2\ Ru$
[M]	728.46
Colour	Yellow
Crystal system	Triclinic
Crystal size/ mm	0.41 x 0.16 x 0.10
Space Group	P-1
a/ Å	9.5667(4)
b/ Å	11.5209(4)
c/ Å	13.2268(5)
α/ °	68.935(2)
β/ °	88.190(2)
γ/ °	86.977(2)
U/ $Å^3$	1358.38(9)
Z	2
D_c/ mgM^{-3}	1.781
F(000)	728
Goodness of fit on F^2	1.078
Conventional R	0.0561
Weighted R	0.1360

Table 3.2 Selected bond lengths (Å) and angles (°) for [(η^6-*p*-cymene)Ru(η^6-1-methyl-3-indolemethyl acetate)]$(PF_6)_2$ (**2a**).

Bond / Angle	Magnitude
Ru (1) – C (2)	2.245 (4)
Ru (1) – C (3)	2.206 (4)
Ru (1) – C (4)	2.200 (3)
Ru (1) – C (5)	2.227 (3)
Ru (1) – C (6)	2.200 (4)
Ru (1) – C (7)	2.211 (4)
Ru (1) – C (11)	2.201 (4)
Ru (1) – C (12)	2.239 (4)
Ru (1) – C (13)	2.326 (3)
Ru (1) – C (14)	2.351 (3)
Ru (1) – C (15)	2.228 (4)
Ru (1) – C (16)	2.187 (4)
C (13) – C (14)	1.443 (5)
C (13) – N (17)	1.368 (5)
C (18)- C (19)	1.358 (6)
C (7) – C (2) – C (3)	117.9 (3)
C (2) – C (3) – C (4)	120.8 (3)
C (3) – C (4) – C (5)	121.0 (3)
C (6) – C (5) – C (4)	117.9 (3)
C (5) – C (6) – C (7)	120.7 (3)
C (2) – C (7) – C (6)	121.6 (3)
C (12) – C (11) – C (16)	120.9 (3)
C (13) – C (12) – C (11)	117.8 (4)
C (12) – C (13) – C (14)	122.2 (3)
C (15) – C (14) – C (13)	118.8 (3)
C (14) – C (15) – C (16)	118.9 (3)
C (11) – C (16) – C (15)	120.8 (4)

A particularly interesting feature is the length of the C (13) – N (17) bond, which, at 1.368 Å, is almost as short as the C (18) – C (19) double bond at 1.358 Å. This can be ascribed to the electron-withdrawing power of the nitrogen atom in the pyrrole ring, which also results in significant lengthening of the C (13) – C (14) bond, making it over 0.02 Å longer than the other C-C bonds within the phenyl ring. An additional important point to note is that the indole ring is tilted by 7.172° along the C (12)-C (15) axis, which is illustrated in Figure 3.5.

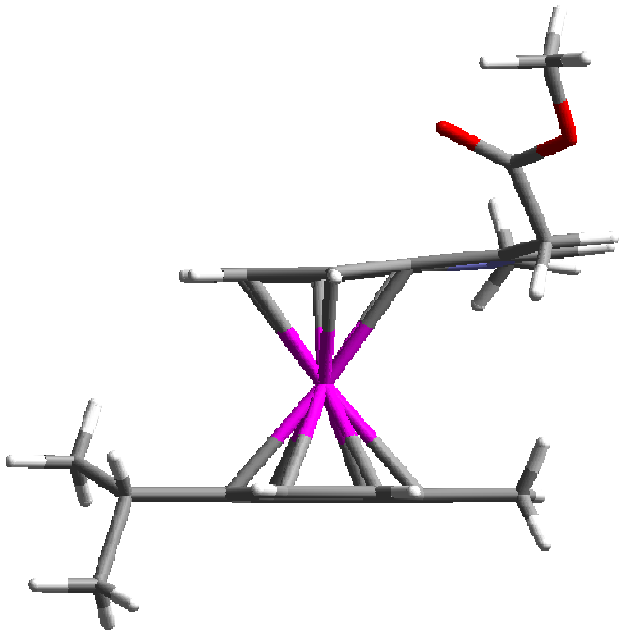

Figure 3.5 Crystal structure of cation in [(η^6-*p*-cymene)Ru(η^6-1-methyl-3-indolemethyl acetate)]$(PF_6)_2$ (**2a**), illustrating the tilting of the indole ligand.

No intermolecular arene ring stacking was observed for this complex. The only significant interactions were the intermolecular hydrogen bonds of length 2.392 Å between O (21) and the H of C (11) on a second molecule (Figure 3.6).

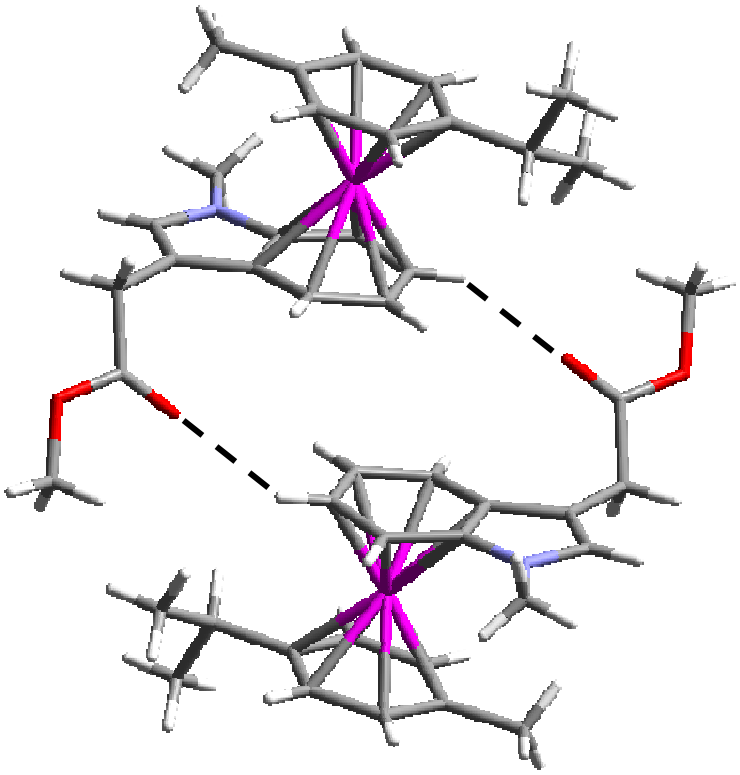

Figure 3.6 Diagram illustrating the intermolecular hydrogen bonds in **2a**.

One of the most interesting features of the crystal structure is that the two molecules present in the unit cell are enantiomers (Figure 3.7) and therefore the complex exists as a 1:1 racemic mixture. These enantiomers are a result of facial chirality, arising due to the asymmetric ligand having two equally possible binding modes, with the methyl group pointing either towards or away from the viewer. No attempt was made to separate these, however it may be possible through diastereomeric resolution with a chiral anion for example.

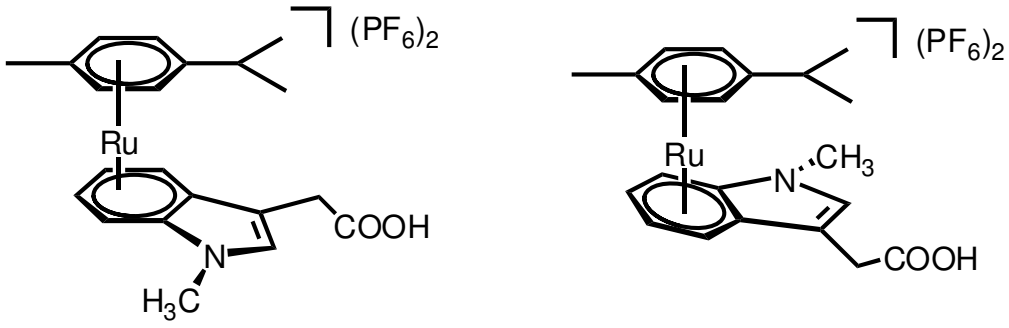

Figure 3.7 Chemical structures of the two possible orientations of the indole ring in **2**, giving rise to enantiomers with facial chirality.

3.3.2.3 pH* dependence

The ^{1}H NMR chemical shifts of the indole α-CH_2 protons of [(η^6-*p*-cymene)Ru(η^6 -1–methylindole–3-acetic acid)]$(PF_6)_2$ (**2**) in D_2O at 298 K were followed with changes in pH* over the range *ca.* 2 to *ca.* 8.5. These were then fitted to the Henderson-Hasselbalch equation (Figure 3.8) to obtain a pK_a* value, which was converted to a pK_a value for the carboxyl group of 3.52. This was repeated for the isolated ligand, which was found to have a considerably higher value of 6.25. The binding of 1-methylindole-3-acetic acid to ruthenium significantly increases the acidity of the carboxyl group by over 2.5 pK units. The results also indicate that the pK_b of the quaternary amide group is well out with the pH range investigated (pK_b < 2).

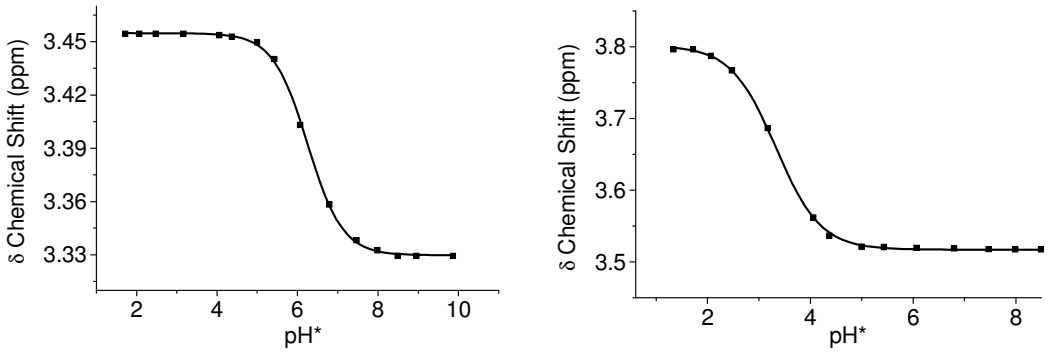

Figure 3.8 Determination of pK_a^* values. Dependence on pH* of the ^{1}H NMR chemical shifts of the α-CH_2 protons of (A) 1-methylindole-3-acetic acid and (B) [(η^6-*p*-cymene)Ru(η^6-1-methylindole-3-acetic acid)](PF_6)$_2$ (**2**). The curves represent the best fits to the Henderson-Hasselbalch equation, from which the pK_a^* and pK_a values were calculated.

3.3.2.4 Stability Studies

The ^{1}H NMR spectra of **2** in 95% H_2O / 5% D_2O at pH 7.04 (10 mM phosphate buffer) were recorded at 310 K at time intervals of 3 h for 48 h followed by a final measurement after 72 h (Figure 3.9). After 6 h, new peaks were observed which appeared to correspond to free 1-methylindole-3-acetic acid (**x**) and a *p*-cymene mono-arene complex (**2m**). These continued to grow in over time with the simultaneous disappearance of the peaks corresponding to the intact bis-arene complex, and after 72 h complete conversion to the new species had taken place. A rate of 2.3×10^{-5} s^{-1} was obtained for the decomposition of **2** by plotting the percentage of the parent species versus time and fitting the data to the appropriate equation for first-order kinetics (Figure 3.10).

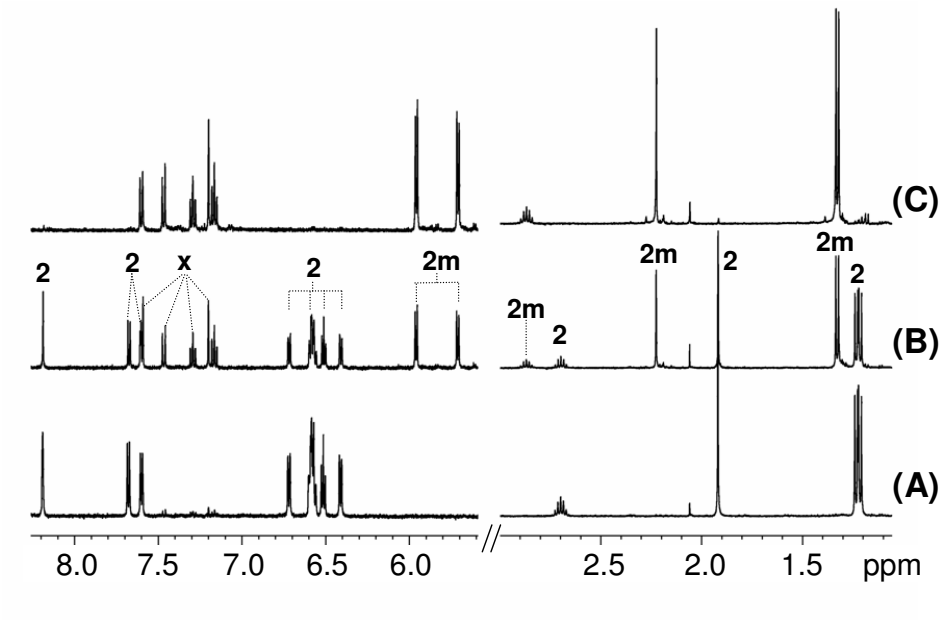

Figure 3.9 Decomposition of [(η^6-*p*-cymene)Ru(η^6-1-methylindole-3-acetic acid)]$(PF_6)_2$ **(2)**. ^{1}H NMR spectra of **2** in 5% D_2O/95% H_2O at 310 K in 10 mM phosphate buffer (pH 7.04) after (A) 0 h, (B) 12 h and (C) 72 h, showing the decrease in intensity of the peaks corresponding to **2** and the increase in intensity of peaks for free 1-methylindole-3-acetic acid (**x**) and a mono-arene species (**2m**).

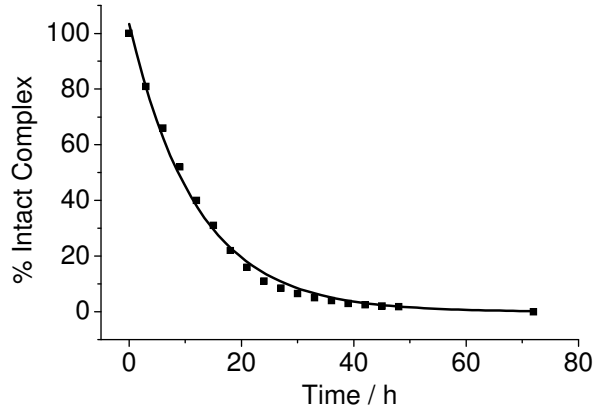

Figure 3.10 Decrease in intensity with time of ^{1}H NMR signals corresponding to [(η^6-*p*-cymene)Ru(η^6-1-methylindole-3-acetic acid)]$(PF_6)_2$ **(2)** in 5% D_2O/95% H_2O at 310 K in 10 mM phosphate buffer (pH 7.04). The curve represents the computer best-fit for a first-order reaction with a rate constant of 2.3×10^{-5} s^{-1}.

Analysis of the ^{1}H NMR reaction mixture at the 12 h time-point by electrospray mass spectrometry revealed three major peaks at m/z 212.6, m/z 390.0 and m/z 463.1, the latter two showing the isotopic pattern for a single ruthenium atom. Mass spectra simulations were carried out to aid identification of these species. M/z 212.6 corresponds to free 1-methylindole-3-acetic acid plus a sodium ion picked up during the ionisation process [$C_{11}H_{11}NO_2Na^+$, M=212.07]. The species responsible for the second peak at m/z 390.0 (**2m**) is most likely to be a mono-arene complex with a single *p*-cymene ligand. Given that the NMR solution contained only **2** and D_2O, it is likely that **2m** contains three bound solvent molecules to fill the coordination sphere of ruthenium. A postulated structure is [$C_{10}H_{15}D_2K_2NaO_3Ru^+$, M=389.95]. The small peak at m/z 463.1 corresponds to **2**, with the acid group having picked up a K^+ ion [$C_{21}H_{24}NO_2RuK^+$, M=463.06], illustrating the presence of some of the original complex. Similar analysis after 72 h revealed that only the m/z 212.6 and m/z 390.0 species were present, consistent with the ^{1}H NMR data that all intact bis-arene complex had been converted to free 1-methylindole-3-acetic acid and **2m**.

These results illustrate that [(η^6-*p*-cymene)Ru(η^6-1-methyl-3-indoleacetic acid)]$(PF_6)_2$ is not stable in solution resulting in the loss of the 1-methylindole-3-acetic acid ligand with time due to solvent molecule attack at the metal centre. In order to investigate this further, the behaviour of **2** in water and a more strongly coordinating solvent, dimethyl sulfoxide (DMSO), was studied by high performance liquid chromatography – electrospray ionisation mass spectrometry (HPLC-ESI-MS). Solutions of **2** in the two solvents were prepared and immediately injected into the HPLC-ESI-MS system. The chromatogram obtained for the complex in H_2O

showed only 1 peak (Figure 3.11) with a mass corresponding to the intact bis-arene complex **2**.

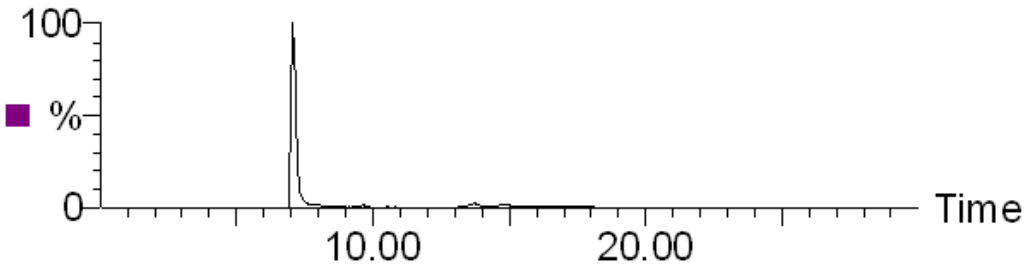

Figure 3.11 HPLC chromatogram of a solution of **2** in H_2O.

The HPLC chromatogram for a solution of **2** in DMSO shows two major peaks (Figure 3.12), neither of which elute at the same time as that observed for the H_2O solution (Figure 3.11). In addition, the mass spectrum for the second eluted peak B (Figure 3.13) shows no ions corresponding to the intact parent complex. DMSO is a strongly coordinating solvent, therefore it is likely that the solvent induced degradation of **2** observed in D_2O by ^1H NMR is accelerated and the mixture is therefore likely to be a number of decomposition products and solvent adducts.

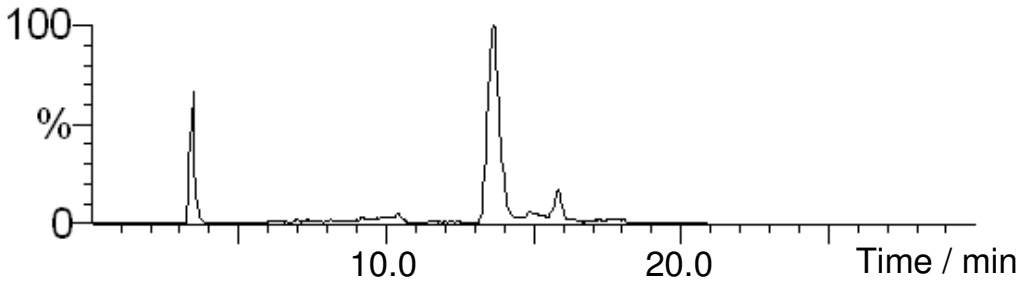

Figure 3.12 HPLC chromatogram for solution of **2** in DMSO.

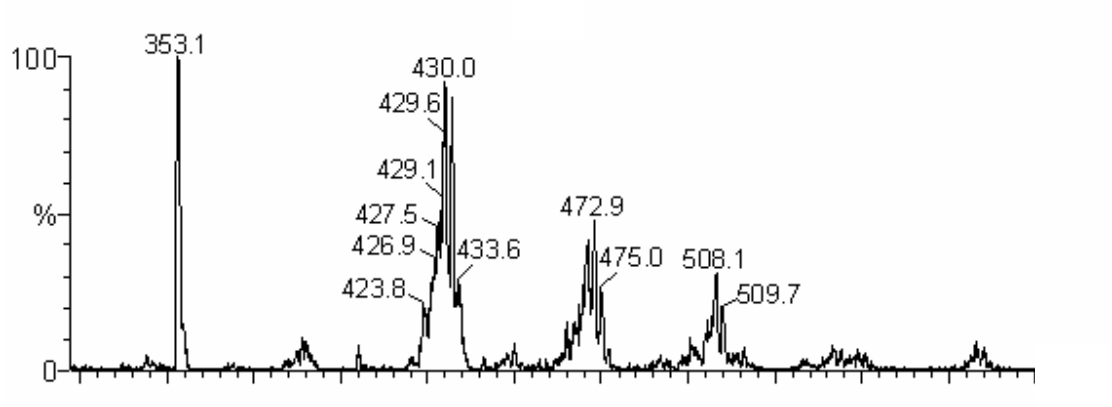

Figure 3.13 Mass spectrum of second eluted HPLC peak (B, Figure 3.12) from a solution of **2** in DMSO.

3.3.2.5 Cytotoxicity Studies

Complex **2** was non-toxic towards both the human ovarian A2780 and human lung A549 cancer cell lines at concentrations up to 100 μM, and therefore it is deemed inactive.

3.4 Discussion

3.4.1 [(η^6-*p*-cymene)Ru(η^6-indole-3-carbinol)](OTf)$_2$ (1)

A detailed review of the chemistry and pharmacology of indole-3-carbinol by Broadbent and Broadbent states that the compound undergoes transformations in stomach acid to form various acid condensation and oligomerisation products, and it is these which are the active components against cancerous cells[7, 9]. However, this instability is not confined to *in vivo*, a number of *in vitro* studies have demonstrated

the formation of at least fifteen oligomers in acidic conditions (Figure 3.14)[22]. This process also occurs slowly at neutral pH with longer oligomer formation favoured as the pH is decreased[23]. The mechanism for these condensation reactions is thought to involve a stable, but highly reactive, benzylic-type carbocation which then attacks positions 2 or 3 of the indole ring of another molecule[24].Varying combinations of sigmatropic shifts and losses of small molecules result in the different products[23].

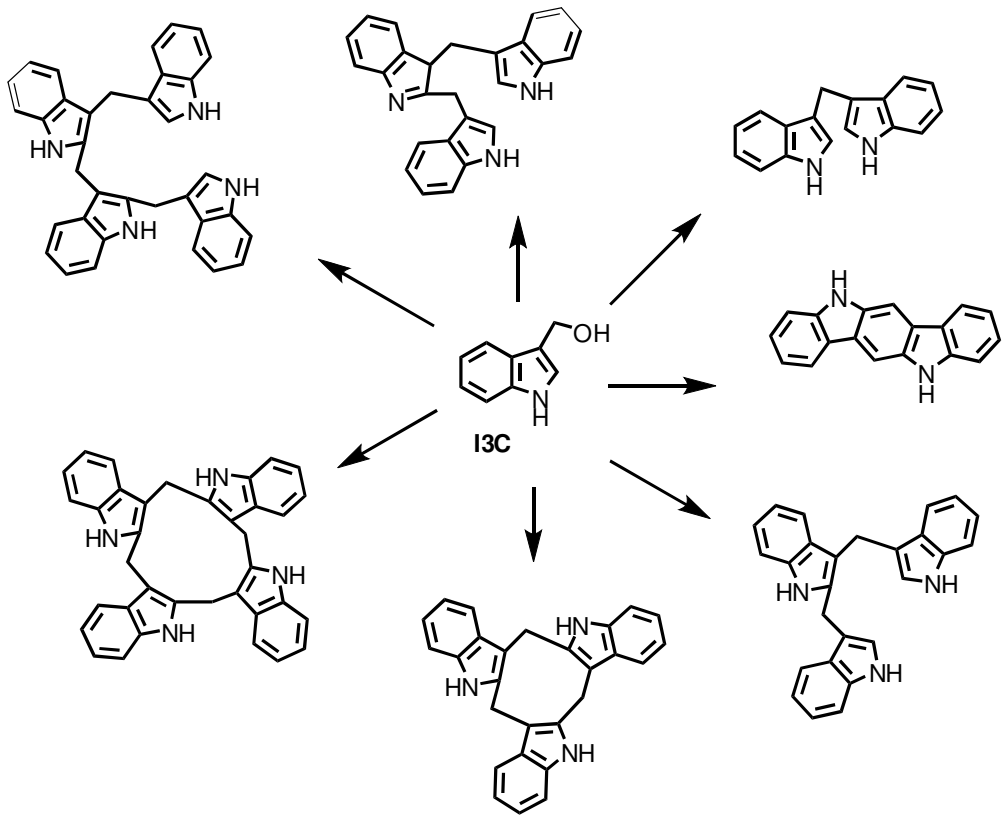

Figure 3.14 The chemical structures of indole-3-carbinol (I3C) and its major acid condensation and oligomerisation products[23].

This clearly explains why initial synthetic attempts using the strong acid trifluoroacetic acid (pK_a 0.3) failed. The use of this solvent is well reported in the literature for the synthesis of bis-arene complexes as it promotes η^6-coordination of the ligand to the metal centre by the protonation of competing σ–donation sites such as carboxylate and amino groups[4, 6]. Improved success was obtained with more neutral solvents such as acetone, but the lack of pure product observed is likely to be due to the formation of both σ– and π–bonded complexes in addition to slow oligomer formation.

In addition to the reactions in acid, indole-3-carbinol is unstable with respect to light and the presence of oxidising agents also accelerates polymerisation[24]. Such contact with light was minimised by the wrapping of reaction vessels in aluminium foil. Although this appeared successful, with solutions turning orange during the reaction and evidence of a precipitate on cooling, reaction work-up under such conditions proved very challenging and in almost every case the reaction mixture turned very dark in colour and the precipitate became very sticky. Schlenk conditions were also employed to minimise contact with air, however on product isolation and analysis rapid absorption of moisture and degradation occurred, as indicated by the ^{1}H NMR spectra obtained.

The observed colour changes on contact with air are also interesting, particularly the development of a purple colour. This may indicate the formation of indigo. Although there is no literature report on such a transformation of indole-3-carbinol, indole is known to be oxidised to a number of indigoid pigments within the body[25]. Figure 3.15 outlines the major pathway and intermediates thought to be generated during

this reaction. Although indigo is a major product it should be noted that a number of other pigments of similar structure are also formed. Due to the high reactivity of [(η^6-*p*-cymene)Ru(η^6-indole-3-carbinol)](OTf)$_2$ (**1**) observed, it is likely that in addition to the oligomerisation discussed, reactions leading to such pigments are also feasible, possibly through air oxidation, thus explaining the colour changes observed. Laboratory preparations of indigo from indoles are also documented[26].

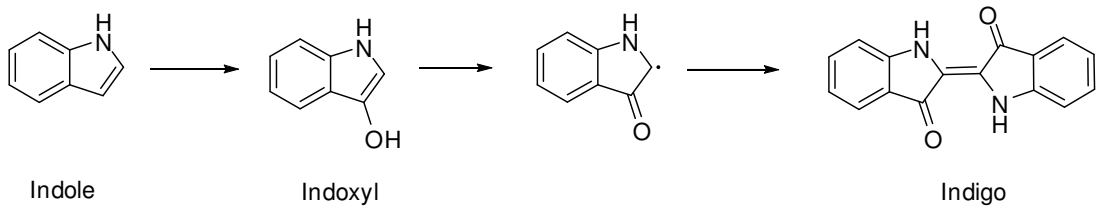

Figure 3.15 Postulated major reaction pathway and intermediates for the *in vivo* generation of indigo from indole.

Although what is known about the chemistry of indole-3-carbinol suggests that it is a very challenging compound to work with, it was hoped that if successful η^6-coordination to ruthenium was achieved, the electronics and properties of the ligand would be sufficiently altered for the product to remain stable. The extensive studies and variety of reaction conditions carried out clearly demonstrate that this is not the case, with evidence for the formation of a number of different species on contact with air or moisture even when bis-arene complex formation appears to have been successful. This instability of [(η^6-*p*-cymene)Ru(η^6-indole-3-carbinol)](OTf)$_2$ **(1)** makes this system unsuitable for further study. Furthermore, it has little potential as an anticancer agent as, in addition to the fact that a pure, stable product could not be

obtained, its high reactivity would make determination of the exact nature of the species being investigated impossible.

3.4.2 [(η^6-*p*-cymene)Ru(η^6 - 1 – methylindole – 3 - acetic acid)](PF_6)$_2$ (2)

3.4.2.1 Synthesis and Structure

[(η^6-*p*-Cymene)Ru(η^6-1-methylindole-3-acetic acid)](PF_6)$_2$ (**2**) was successfully synthesised using the method of Bennett and Matheson[27], employing trifluoroacetic acid as the reaction solvent. In addition to accurate mass spectrometry and elemental analysis data, η^6 - coordination via the phenyl ring to generate a bis-arene complex was also confirmed by the characteristic upfield shift[19] of the signals for the aromatic protons of 1-methylindole-3-acetic acid on metal binding combined with the downfield shift of the aromatic protons of *p*-cymene relative to the half-sandwich starting material[6].

3.4.2.2 X-ray Crystallography

The crystal structure of the methyl ester [(η^6-*p*-cymene)Ru(η^6-1-methyl-3-indolemethyl acetate)](PF_6)$_2$ (**2a**) confirms the expected bis-arene structure with two essentially parallel η^6-arene ligands. The angle between the ruthenium and the centre of each ring is 179.0° which is comparable to that observed for similar complexes [19, 20].

The observed tilting of the indole ring by 7.172° along the C (12)-C (15) axis is interesting and indicates some loss of η^6-coordination to the ruthenium. This is further corroborated by the fact that the Ru – C(13) and Ru – C(14) are 2.326(3) Å and 2.351(3) Å respectively, significantly longer than the Ru – C distances for the other coordinated indole carbon atoms (2.187 – 2.239 Å). The observed intermolecular hydrogen bonds in the crystal structure of **2a** could be a contributory factor to this. However, the main origin is thought to be the fact that the two ring junction carbons (C(13) and C(14)) are not able to π-bond as effectively with the metal as the other ring carbons as their π–electrons are involved in bonding to three other carbons instead of two[28]. This phenomenon, also known as 'ring slippage', has been shown for other complexes containing indole rings, for example, [(η^6-*p*-cymene)Ru(η^6-5-OTrpOH)](OTf)$_2$ shows a tilting angle of 12.4°[5], in addition to a range of other metal-arene systems[28].

A consequence of this ring-tilting may be the creation of a space large enough for solvent molecules to attack the ruthenium centre and form new species and it is therefore a possible explanation for the observed arene loss for this complex in solution. Arene displacement reactions are thought to occur by attack of the external (solvent) ligand after η^6-η^4 dissociation of the arene[28]. It therefore follows that for complexes with coordinated arene rings which are tilted, such as **2**, arene lability is enhanced due to the greater accessibility of the metal centre[29].

Indole and its derivatives are generally thought of as electron-rich heterocycles due to the involvement of the nitrogen lone pair in the aromatic π–system. The electron withdrawing nature of the 5-membered pyrrole ring is exemplified in the crystal

structure by the shortening of the C (13) – N (17) bond, implying that the benzene ring component of the indole ligand is electron-poor compared to the *p*-cymene ligand which contains only electron-donating methyl substituents. This, combined with the observed 'ring slippage', is likely to be the reason why the *p*-cymene ligand is closer to the metal by over 0.05 Å compared to 1-methylindole-3-acetic acid. The Ru-cymene$_{(centroid)}$ distance of 1.707 Å is very similar to that observed for [(η^6-*p*-cymene)Ru(η^6-1-methylindole)](OTf)$_2$ of 1.706 Å[19] and both are significantly longer than the average distance in other (cymene)Ru(arene) derivatives of 1.678 Å[30]. Similarly, the Ru-indolemethyl acetate$_{(centroid)}$ distance of 1.757 Å for **2a** is comparable to that of the indole complex (1.761 Å)[19]. A parallel trend was observed for [(η^6-*p*-cymene)Ru(η^6-1–methylindoline)](BPh$_4$)$_2$ where Ru-cymene$_{(centroid)}$ = 1.730 Å and Ru-indole$_{(centroid)}$ = 1.773 Å[20].

Interestingly, the facial chirality observed for **2a** is also well documented for other closely related systems. Most show enantiomer ratios of 1:1 in the crystal structures[4, 20] indicating no preference for one isomer over the other, however in one case of facial chirality preferential crystallisation of one diastereomer was reported[5].

3.4.2.3 pH* Dependence

The pK_a value for the carboxyl group of 1-methylindole-3-acetic acid is significantly lowered from 6.25 to 3.52 on metal binding. This trend in increased acidity is consistent with many other similar bis-arene complexes in the literature[4, 5, 20]. However, this change will have no effect on the nature of the species at physiological pH.

The NH group on an indole ring is weakly acidic with a pK_a value of 16.97, with indole-3-acetic acid having a very similar value of 16.90[31], although much enhanced acidity is observed over ammonia (pK_a ~22)[7]. The bascitiy of the nitrogen atom is accordingly reduced compared to ammonia (pK_b = -3.6, cf. 4.75). This is a result of indole being a π–rich heterocycle with delocalisation of the nitrogen lone pair into the π–system. This leads to enhanced π–electron density on the carbon atoms and reduced density on the nitrogen[7]. Since the nitrogen is methylated in **2**, this group would be expected to behave as a base. However, even with the electron-donating properties of the methyl group, the enhanced acidity resulting from metal coordination would most likely result in a pK_b value well below -3.6 and hence its measurement was not possible under the conditions studied.

3.4.2.4 Stability Studies

The observed loss of the 1-methylindole-3-acetic acid arene ligand from **2** in solution is unusual. In the literature, there are several examples of photochemical displacement of an η^6-arene from ruthenium for both mono- and bis-arene systems, [32, 33] but such thermal displacement under mild conditions is much more rare [34, 35].

The observed arene loss can be rationalised not only by considering the loss of η^6-coordination, implied by the crystal structure, but also by the nature of the bonding of the arene to Ru(II), which is strengthened by increasing the amount of π–electron density on the arene ligand which can be donated to the metal centre[29]. Indole and its derivatives have a tightly bound and stable π-electron system and disruption of this is unfavourable. Therefore, in [(η^6-*p*-cymene)Ru(η^6-1-methylindole-3-acetic

acid)]$(PF_6)_2$ (**2**), the indole-3-acetic acid ligand is less tightly bound due to competition between the ruthenium and the π–system of the heterocycle for the π–electron density.

3.4.2.5 Cytotoxicity

The non-toxic nature of **2** towards both the human ovarian A2780 and human lung A549 cancer cell lines at concentrations up to 100 μM is unlikely to provide a general guide to the toxicity of this complex. The cytotoxicity studies involve dissolution of the complexes in a DMSO/water mixture prior to addition to the cells. The results obtained from the stability studies on this complex clearly show that **2** would break down in such a solvent mixture and therefore it is most likely that it is not the intact bis-arene complex which is being tested but a number of decomposition products.

3.5 Conclusions

Two novel bis-arene ruthenium complexes of indole derivatives, [(η^6-*p*-cymene)Ru(η^6-indole-3-carbinol)]$(OTf)_2$ (**1**) and [(η^6-*p*-cymene)Ru(η^6-1-methyl-indole-3-acetic acid)]$(PF_6)_2$ (**2**) were synthesised and studied in this work. It was hoped that the known biological properties of the ligands would lead to novel metal complexes with anticancer properties.

[(η^6-*p*-Cymene)Ru(η^6-indole-3-carbinol)]$(OTf)_2$ (**1**) was found to be highly reactive, with rapid decomposition of the complex into a wide range of oligomeric products

occurring on contact with air and in solution. A variety of synthetic conditions were investigated, none of which resulted in stable complex formation, and it was not possible to isolate the desired product.

[(η^6-*p*-Cymene)Ru(η^6-1-methyl-indole-3-acetic acid)](PF_6)$_2$ (**2**) formed an air-stable bis-arene complex with ruthenium, however loss of the indole ligand occurs in solution. The rate of this arene loss is 2.3×10^{-5} s^{-1} in aqueous solution and increases dramatically in more strongly coordinating solvents such as DMSO. Coordination of the indole derivative to the metal centre resulted in a dramatic increase in the acidity of the ligand, as shown by the decrease in pK_a of the carboxyl group from 6.25 to 3.52. The X-ray crystal structure of **2** was obtained as the methyl ester (**2a**) and it was found that the two molecules in the unit cell were enantiomers as a result of facial chirality. The indole ring is tilted by 7.172° in the solid state, implying some degree of loss of η^6-coordination. This, if also present in solution, may be a contributing factor to the observed dissociation of the ligand.

The racemic mixture of **2** was found to be non-toxic against both the A2780 breast cancer and A549 lung cancer cell lines. However, due to the time dependent breakdown of the compound, it is likely that a mixture of products were being tested and therefore no direct conclusions about the activity of the intact complex can be made.

This work demonstrates that although amino acids and their derivatives readily form stable bis-arene complexes with ruthenium[5, 6, 19], very minor changes to their electronic structure (replacement of H by Me for example) can drastically affect their properties and reactivity, and careful consideration of the whole system is necessary.

Unfortunately, due to the highly reactive nature of both complexes studied here, it is unlikely that either would be suitable for such an application. However, if the rate of loss of 1-methylindole-3-acetic acid from the metal centre could be controlled, it is possible to envisage the metal acting as a carrier, with delivery of the ligand to specific sites within the body, imparting novel properties to the complex.

3.6 References

[1] C. Orvig, M. J. Abrams, *Chem. Rev.,* **1999**, *99*, 2201.

[2] K. Severin, R. Bergs, W. Beck, *Angew. Chem., Intl Ed.,* **1998**, *37*, 1635.

[3] W. S. Sheldrick, S. Heeb, *J. Organomet. Chem.,* **1989**, *377*, 357.

[4] R. Stodt, S. Gencaslan, A. Frodl, C. Schmidt, W. S. Sheldrick, *Inorg. Chim. Acta,* **2003**, *355*, 242.

[5] A. Schluter, K. Bieber, W. S. Sheldrick, *Inorg. Chim. Acta,* **2002**, *340*, 35.

[6] J. M. Wolff, W. S. Sheldrick, *J. Organomet. Chem.,* **1997**, *531*, 141.

[7] T. A. Broadbent, H. S. Broadbent, *Curr. Med. Chem.,* **1998**, *5*, 337.

[8] W.-R. Chao, D. Yean, K. Amin, C. Green, L. Jong, *J. Med. Chem.,* **2007**, *50*, 3412.

[9] T. A. Broadbent, H. S. Broadbent, *Curr. Med. Chem.,* **1998**, *5*, 469.

[10] M. P. d. Melo, T. M. d. Lima, T. C. Pithon-Curi, R. Curi, *Toxicol. Lett.,***2004**, *148*, 103.

[11] S. Furukawa, K. Usuda, M. Abe, I. Ogawa, *J. Toxicol. Sci.,* **2005**, *30*, 165.

[12] L. K. Folkes, S. Rossiter, P. Wardman, *Chem. Res. Toxicol.,* **2002**, *15*, 877.

[13] L. K. Folkes, M. F. Dennis, M. R. L. Stratford, L. P. Candeias, P. Wardman, *Biochem. Pharmacol.,* **1999**, *57*, 375.

[14] L. K. Folkes, P. Wardman, *Biochem. Pharmacol.,* **2001**, *61*, 129.

[15] L. K. Folkes, P. Wardman, *Cancer Res.,* **2003**, *63*, 776.

[16] G. K. Sandhu, N. Sharma, *Appl. Organomet. Chem.,* **1993**, *7*, 39.

[17] J.-H. Yang, Y.-S. Han, M. Park, T. Park, S.-J. Hwang, J.-H. Choy, *Chem. Mater.,* **2007**, *19*, 2679.

[18] W. S. Sheldrick, A. Gleichmann, *J. Organomet. Chem.,***1994**, *470*, 183.

[19] S. Chen, V. Carperos, B. Noll, R. J. Swope, M. R. DuBois, *Organometallics,* **1995**, *14*, 1221.

[20] S. Chen, L. Vasquez, B. C. Noll, M. R. DuBois, *Organometallics,* **1997**, *16*, 1757.

[21] Origin, 7.5 Ed., OriginLab Corporation, Northampton, **2006**.

[22] M. J. Anderton, R. Jukes, J. H. Lamb, M. M. Manson, A. Gescher, W. P. Steward, M. L. Williams, *J. Chromatog., B,* **2003**, *787*, 281.

[23] K. R. Grose, L. F. Bjeldanes, *Chem. Res. Toxicol.,* **1992**, *5*, 188.

[24] G. Brandi, M. Paiardini, B. Cervasi, C. Fiorucci, P. Filippone, C. De Marco, N. Zaffaroni, M. Magnani, *Cancer Res.,* **2003**, *63*, 4028.

[25] E. M. J. Gillam, L. M. Notley, H. Cai, J. J. De Voss, F. P. Guengerich, *Biochemistry,* **2000**, *39*, 13817.

[26] Y. Yamamoto, U. Takaki, S. Aoki, I. Hara, (Mitsui Toatsu Chemicals, Inc., Japan), Eur. Pat. Appl., **1990**, 8pp.

[27] M. A. Bennett, T. W. Matheson, *J. Organomet. Chem.,* **1979**, *175*, 87.

[28] E. L. Muetterties, J. R. Bleeke, E. J. Wucherer, T. Albright, *Chem. Rev.,* **1982**, *82*, 499.

[29] I. S. Butler, A. A. Ismail, *Inorg. Chem.* **1986**, *25*, 3910.

[30] F. B. McCormick, D. D. Cox, W. B. Gleason, *Organometallics,* **1993**, *12*, 610.

[31] G. Yagil, *Tetrahedron,* **1967**, *23*, 2855.

[32] T. Karlen, A. Hauser, A. Ludi, *Inorg. Chem.,* **1994**, *33*, 2213.

[33] S. W. Magennis, A. Habtemariam, O. Novakova, J. B. Henry, S. Meier, S. Parsons, I. D. H. Oswald, V. Brabec, P. J. Sadler, *Inorg. Chem.,* **2007**, *46*, 5059.

[34] D. A. Freedman, D. E. Janzen, K. R. Mann, *Inorg. Chem.,* **2001**, *40*, 6009.

[35] S. J. Dougan, M. Melchart, A. Habtemariam, S. Parsons, P. J. Sadler, *Inorg. Chem.,* **2006**, *45*, 10882.

Chapter 4 Ruthenium and Osmium Complexes Containing Aspartame

4.1 Introduction

In Chapter 3, the potential of binding two amino acid derivatives to ruthenium in order to generate metal complexes with applications as anticancer agents was discussed. Here, the feasibility of extending work on such a class of ligands is investigated by exploring the synthesis and properties of ruthenium and osmium complexes of a dipeptide, α-*L*-aspartyl-*L*-phenylalanine methyl ester, aspartame.

There are far fewer examples of bis-arene metal complexes containing peptides compared to single amino acids, however a limited number of systems have been investigated[1, 2]. Recently, this work has been extended to small proteins where selective binding of a ruthenium organometallic fragment to a phenylalanine residue of secretin via η^6-coordination in aqueous media was achieved[3]. Synthesis of π–bound peptides may be achieved by direct binding to the metal or through peptide synthesis on the side-chain of a metal-bound amino acid[4]. This leads to interesting synthetic applications if the organometallic fragment facilitates novel couplings and may then be removed at the end of the reaction[5].

Aspartame (α-*L*-aspartyl-*L*-phenylalanine methyl ester, Figure 4.1) is a low-calorie sweetener[6]. It is a white, odourless powder with a sweetness potency of up to 200 times that of sucrose[7]. On consumption it is rapidly converted into a number of decomposition products and, eventually, into its three constituents: aspartic acid, phenylalanine and methanol[8]. Aspartame is thought to interact with the sweet taste receptor *via* three important functionalities: the carboxylate and amino groups through electrostatics and hydrogen bonding, and the aromatic ring via hydrophobic interactions[9].

In addition to these well studied biological reactions of aspartame, it has also been shown to interact with DNA *in vitro* through electrostatic binding between the amino group and the phosphate backbone of DNA in addition to a partial intercalation of the aromatic ring[10]. Although there have been a number of reports associating aspartame intake with an increased risk of cancer, a recent review of a variety of clinical studies has found no link between the two and that at current levels of consumption, the sweetener is harmless to humans[11]. There is no known anticancer activity associated with aspartame.

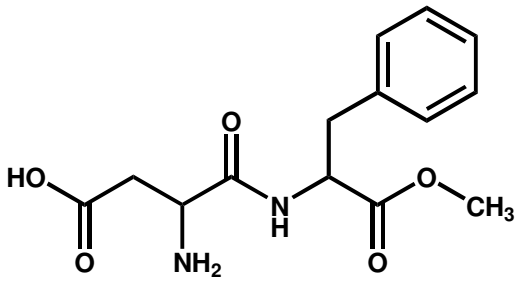

Figure 4.1 Chemical structure of aspartame (α-*L*-aspartyl-*L*-phenylalanine methyl ester)

Reports on metal coordination complexes of aspartame are at present limited to metals such as copper, nickel and zinc, in which binding occurs through the carboxylate and amino groups[12, 13]. To date, there have been no investigations into whether or not these metal complexes retain any of the activity inherent to aspartame. This chapter describes the synthesis and characterisation of complexes of ruthenium(II) and osmium(II) containing aspartame bound through η^6-coordination

and investigations of reactions of potential importance for their biological activity. In particular, their interaction with the sweet taste receptor is studied.

4.2 Experimental

4.2.1 Materials

The preparation of the starting materials $[(\eta^6\text{-}p\text{-cymene})RuCl_2]_2$ and $[(\eta^6\text{-}p\text{-cymene})OsCl_2]_2$ is reported in Chapter 2. Aspartame was purchased from Supelco Analytical, ascorbic acid from Alfa Aesar and silver trifluoromethanesulfonate (AgOTf) (≥ 99%) from Sigma-Aldrich. Acetone was dried by reflux over K_2CO_3 prior to use.

4.2.2 Synthesis

$[(\eta^6\text{-}p\text{-cymene})Ru(\eta^6\text{-aspartame})](OTf)_2$ (3) $[(\eta^6\text{-}p\text{-cymene})RuCl_2]_2$ (0.13 g, 0.2 mmol) was stirred in dry acetone (7 mL) with AgOTf (0.22 g, 0.8 mmol) for 30 min at ambient temperature. Removal of the AgCl precipitate by filtration was carried out under Schlenk conditions yielding a clear red solution. Excess solvent was removed under vacuum, affording a red oily residue of the intermediate $[(\eta^6\text{-}p\text{-cymene})Ru(acetone)_3](OTf)_2$. A solution of aspartame (0.12 g, 0.4 mmol) in trifluoroacetic acid (6 mL) was added to the Schlenk flask and the clear red mixture stirred for 18 h at 323 K. After cooling, addition of diethyl ether, to the resulting cloudy orange solution, resulted in the formation of a yellow crystalline precipitate which was filtered, washed with ether and dried *in vacuo*. (Yield: 185 mg, 55.9%).

Anal. Found %C = 38.29; %H = 4.10; %N = 3.55. Calc. for $C_{26}H_{32}N_2O_{11}RuS_2F_6$ (M = 827.73): %C = 37.73; %H = 3.87; %N = 3.39. ESI MS: Calc. for $C_{26}H_{32}N_2O_{11}RuS_2F_6$ $[M+H]^+$ *m/z* 829.04, found 828.73. ^{1}H NMR, 600MHz (D_2O): δ 1.32 (d, 6H, cymene), 2.49 (s, 3H, cymene), 2.95 (sp, 1H, cymene), 3.07 (m, 3H, Asp), 3.35 (dd, 1H, Asp), 3.78 (s, 3H, Asp), 4.36 (dd, 1H, Asp), 4.88 (dd, 1H, Asp) 7.00 (m, 8H, cymene + Ph), 7.14 (d, 1H, cymene).

[(η^6-*p*-cymene)Os(η^6-aspartame)](OTf)$_2$ (4) [(η^6-*p*-cymene)$OsCl_2]_2$ (0.051 g, 0.06 mmol) was stirred in dry acetone (3 mL) with AgOTf (0.069 g, 0.24 mmol) for 30 min at ambient temperature. Filtration of the AgCl precipitate yielded a clear orange solution. Excess solvent was removed in vacuum, affording an orange oily residue of the intermediate [(η^6-*p*-cymene)Os(acetone)$_3$](OTf)$_2$. Aspartame (0.038 g, 0.12 mmol) in trifluoroacetic acid (5 mL) was then added to the [(η^6-*p*-cymene)Os(acetone)$_3$](OTf)$_2$ and the clear orange mixture stirred for 20 h at 333 K. After cooling, diethyl ether was added to the resulting yellow solution, to form a yellow/white powder which was filtered and washed with diethyl ether. (Yield: 43 mg, 39.4%)

Anal. Found %C = 34.57; %H = 3.66; %N = 3.59. Calc. for $C_{26}H_{32}N_2O_{11}OsS_2F_6$ (M = 916.6): %C = 34.07; %H = 3.49; %N = 3.06. ESI MS: Calc. for $OsC_{24}H_{31}N_2O_5^+$ [M –H - $2CF_3SO_3$] $^+$ *m/z* 619.19, found 619.20. ^{1}H NMR, 600 MHz (D_2O): δ 1.34 (d, 6H, cymene), 2.29 (s, 3H, cymene), 2.74 (sp, 1H, cymene), 3.00 (m, 4H, Asp), 3.72 (s, 3H, Asp), 4.30 (dd, 1H, Asp), 4.73 (dd, 1H, Asp), 7.30 (m, 9H, cymene + Ph).

4.2.3 Methods

4.2.3.1 pH measurements

pH and pH* values were measured at *ca.* 298 K directly in the NMR tube as described in Chapter 2.

4.2.3.2 Calculation of pK_a Values

For determination of pK_a* values (pK_a values determined for D_2O solutions), the pH* values of the solutions of aspartame and complexes **3** and **4** in 5% MeOD-d_4/95% D_2O were varied from *ca.* 2 to *ca.* 11 by the addition of dilute NaOD and $DClO_4$. ^1H NMR spectra were recorded and chemical shifts plotted against pH*. The pH* titration curves were fitted, using the program ORIGIN 7.5[14], to the modified Henderson-Hasselbalch equation appropriate for two pK_a^* values[15] where δ_{obs} is the chemical shift at a given pH and $\delta_{HH'A}$, $\delta_{H'A}$- and δ_{A2}- are the chemical shifts at low, intermediate and high pH respectively.

For the (de)protonation: $HH'A \rightleftharpoons H^+ + H'A^- \rightleftharpoons H'^+ + A^{2-}$

$$\delta_{obs} = \delta_{HH'A} + (\delta_{H'A^-} - \delta_{HH'A}) \times \frac{10^{(pH^* - pK_{a1}^*)}}{1 + 10^{(pH^* - pK_{a1}^*)}} + (\delta_{A2-} - \delta_{H'A-}) \times \frac{10^{(pH^* - pK_{a2}^*)}}{1 + 10^{(pH^* - pK_{a2}^*)}}$$

The pK_a* values were converted to pK_a values by the use of the equation pK_a = 0.929pK_a* + 0.42, as suggested by Krezel and Bal[16], for comparison with related values in the literature.

4.2.3.3 Stability Studies

Solutions of aspartame, **3** and **4** in 5% MeOD-d_4/5% D_2O/90% H_2O at pH 7.4 (10 mM phosphate buffer) containing 1% dioxane as an internal reference were prepared and ^{1}H NMR spectra recorded at 310 K at time intervals of 0.5 h for 24 h. The percentage conversion of aspartame to 3,6-dioxo-5-phenylmethylpiperazine acetic acid (diketopiperazine, DKP) at a particular time period was determined by peak-integration relative to the internal reference, assuming integration at a time of 0 h corresponded to 0%. The rate of the reaction observed was obtained by plotting these percentages *versus* time and fitting the data to the appropriate equation for first-order kinetics using the program ORIGIN 7.5[14].

4.2.3.4 Electrochemistry

Electrochemistry was carried out using the standard method described in Chapter 2. Cyclic voltammetry was carried out on solutions of aspartame in 0.1 M tetrabutylammonium tetrafluoroborate ($TBABF_4$) in *N,N*-dimethylformamide (DMF) with a sweep width of between +2 and -2 V and with sweep rates of between 0.1 and 1 Vs^{-1}. Differential pulse polarography was carried out on analogous solutions of complexes **3** and **4** over the same potential range due to its enhanced sensitivity[17] which allowed each redox process to be observed at lower concentrations.

4.2.3.5 Reactions with Ascorbate

Solutions of aspartame, **3** and **4** at 100 μM in D_2O at pH 7.04 (10 mM phosphate buffer) containing 1% dioxane as an internal reference were prepared and the ^1H NMR spectra recorded at 310 K. Aliquots of a solution of ascorbic acid in D_2O were added at a number of different excess concentrations (5-50 equivalents) and the ^1H NMR spectra re-recorded at time intervals of 0.5 h for 24 h. The rate of the reaction observed for **3** was obtained by plotting the decrease in intensity of a number of peaks (relative to internal reference) *versus* time and fitting the data to the appropriate equation for pseudo-first order kinetics using the program ORIGIN 7.5[14].

4.2.3.6 Cytotoxicity Testing

Cytotoxicity assays for **3** were performed against human ovarian A2780 and human lung A549 cancer cell lines by Mr Daniel Cole and colleagues at Oncosense Ltd, MMI group, Cambridge, UK as described in Chapter 2.

4.2.3.7 Heterologous Expression to Monitor Interaction with Sweet Taste Receptor

The ability of **3** and **4** to interact with the human sweet taste receptor was monitored using the following assay by Dr Marcel Winnig and colleagues at The German Institute of Human Nutrition, Nuthetal, Germany. The complementary DNAs for hTAS1R2 and hTAS1R3 were transiently transfected into HEK293T cells stably

expressing the chimeric G-protein subunit Gα16gust44[18] using Lipofectamine 2000 (Invitrogen) [19]. 4 h post transfection, Dulbecco's modified Eagle's medium (DMEM) was replaced by low-glucose DMEM supplemented with GlutaMAX and 10% dialyzed foetal bovine serum (FBS, Invitrogen). After an additional 24 h, cells were loaded for 1 h with the calcium-sensitive dye Fluo4-AM (2 μg/mL in DMEM, Molecular Probes). Cells were washed 3 times with solution C1 (130 mM NaCl, 5 mM KCl, 10 mM HEPES, 2 mM $CaCl_2$, and 5 mM Glucose, pH 7.4). The aspartame complexes were dissolved in C1 solution. Calcium mobilisation upon stimulation was monitored by an automated fluorometric imaging plate reader (FLIPR, Molecular Devices) and the calcium signals were corrected for the response of mock transfected cells.

4.3 Results

4.3.1 Synthesis and Structure

Both the ruthenium(II) and osmium(II) bis-arene complexes containing aspartame were synthesised in good yields from the corresponding chlorido-bridged dimers, $[(\eta^6\text{-}p\text{-cymene})MCl_2]_2$ (M = Ru/Os), and were characterised using ^1H NMR spectroscopy, ESI-MS and elemental analysis. η^6 - coordination via the phenyl ring was also confirmed by the characteristic upfield shift of the signals for the aromatic protons of aspartame on metal binding. These data are consistent with the sandwich structures of complexes **3** and **4** shown in Figure 4.2.

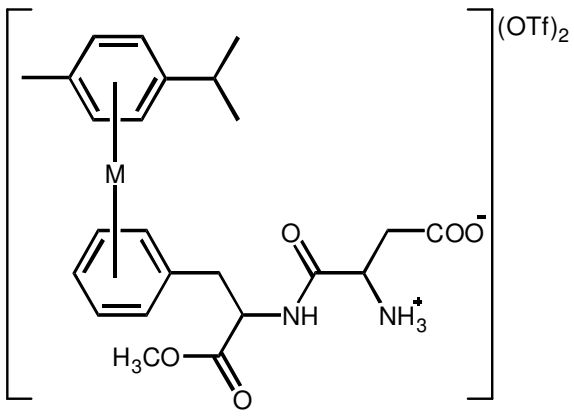

Figure 4.2 The chemical structure of the metal aspartame sandwich complexes **3** (M = Ru) and **4** (M = Os)**.**

4.3.2 pH* dependence and pK_a values

The ^{1}H NMR chemical shifts of the α-CH and β-CH_2 protons of the aspartic acid residue of aspartame at 298 K in 5% MeOD-d_4/95% D_2O were followed with changes in pH* over the range 2-11. This procedure was repeated for the ruthenium and osmium complexes and the data for those peaks with the most significant shifts were fitted to the Henderson-Hasselbalch equation (Figure 4.3) to obtain pK_a* values. These were converted to pK_a values of 3.45, 3.10 and 2.94 for the carboxyl groups, and 7.81, 7.32, and 7.24 for the amino groups of aspartame, **3**, and **4,** respectively (Table 4.1). Importantly, the binding of aspartame to Ru or Os *via* the phenyl group lowers the pK_a values of both the carboxyl and amino groups significantly (by *ca.* 0.5 units).

Table 4.1 pK_a values for aspartame, ruthenium complex **3** and osmium complex **4** determined from NMR pH titration data. Errors in the last digit are shown in brackets.

Compound	COOH	NH_3^+
Aspartame	3.45(1)	7.81(4)
3	3.10(1)	7.32(3)
4	2.94(1)	7.24(3)

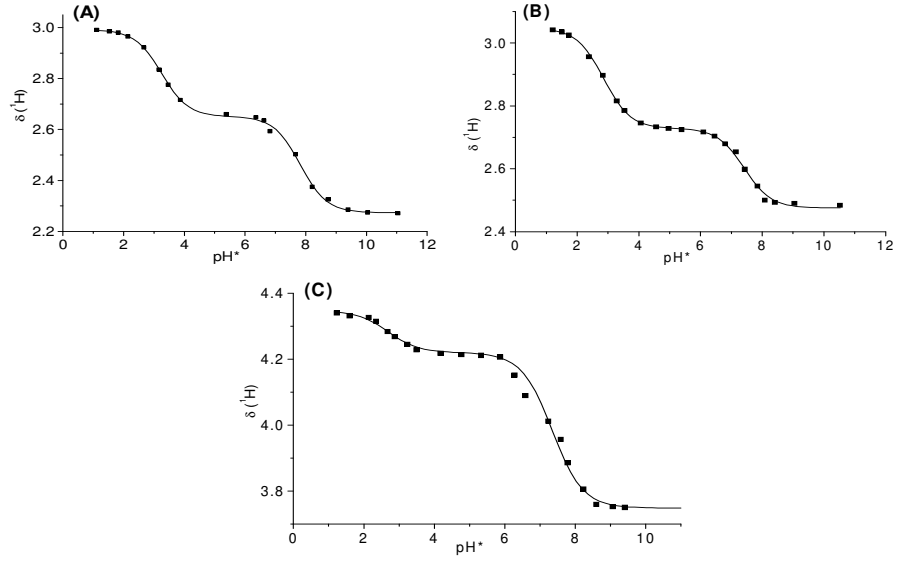

Figure 4.3 Determination of pK_a^* values. Dependence on pH* of the ^{1}H NMR chemical shifts of the α-proton of (A) aspartame, (B) [(η^6-*p*-cymene)Ru(η^6-aspartame)]$^{2+}$ (**3**), and β–protons of (C) [(η^6-*p*-cymene)Os(η^6-aspartame)]$^{2+}$ (**4**). The curves represent the best fits to the Henderson-Hasselbalch equation for two pK_a values and the pK_a^* values to which they correspond were converted to the pK_a values shown in Table 4.1.

4.3.3 Stability Studies

Aspartame is known to degrade in aqueous solution[8]. Under physiologically-relevant conditions (310 K, pH 7.4), the primary step in this degradation is considered to be the formation of 3,6-dioxo-5-phenylmethylpiperazine acetic acid (diketopiperazine, DKP) via the intramolecular cyclisation reaction outlined in Scheme 4.1[20].

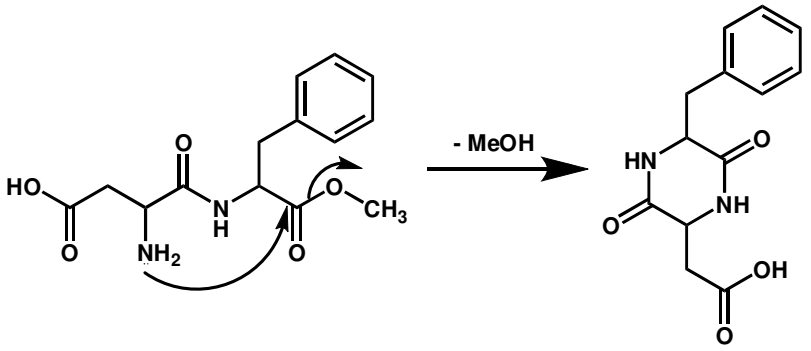

Scheme 4.1 Mechanism for the conversion of aspartame to DKP through an intramolecular cyclisation reaction

The behaviour of aspartame and the Ru and Os complexes under such conditions was monitored in 5% MeOD-d_4/5% D_2O/90% H_2O, 10 mM phosphate buffer (pH 7.4) solutions using ^1H NMR spectroscopy over a 24 h period. All spectra showed growth of a peak for free methanol and disappearance of the signal for the OMe group of bound aspartame over this time (aspartame spectra shown in Figure 4.4), in accordance with the proposed mechanism. Analysis of ^1H NMR peak integrals allowed the percentage conversion of aspartame to DKP to be plotted *versus* time (Figure 4.5). The resultant data were fitted to first-order kinetics from which rates and half-lives for the degradation were obtained. A dramatic increase in rate constant from 0.12 h^{-1} for aspartame to 0.36 h^{-1} for **3** and 0.43 h^{-1} for **4** was observed. It is interesting that osmium has a more pronounced effect on this pathway (by 1.2 fold).

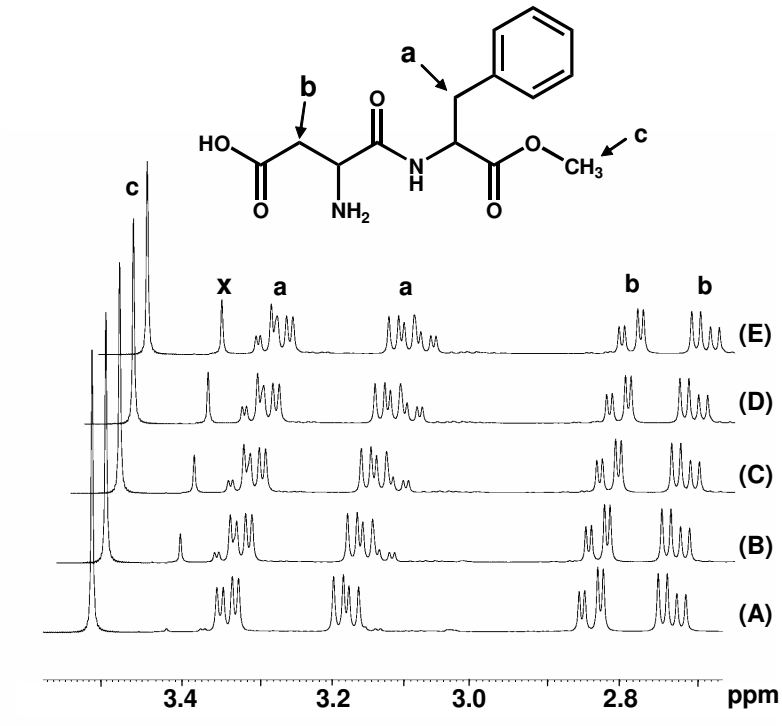

Figure 4.4 Conversion of aspartame into DKP. ^{1}H NMR spectra of aspartame in 5% MeOD-d_4/5% D_2O/90% H_2O at 310 K in 10 mM phosphate buffer (pH 7.4) after (A) 0 h, (B) 4 h, (C) 8 h, (D) 12 h and (E) 16 h, showing the decrease in intensity of the peak for bound OMe at 3.51 ppm (**c**) and the increase in intensity of the peak for free MeOH (**x**). A small downfield shift of *ca.* 0.02 ppm for peaks between 2.7 and 2.9 ppm is also observed. Peak labels correspond to the structure shown.

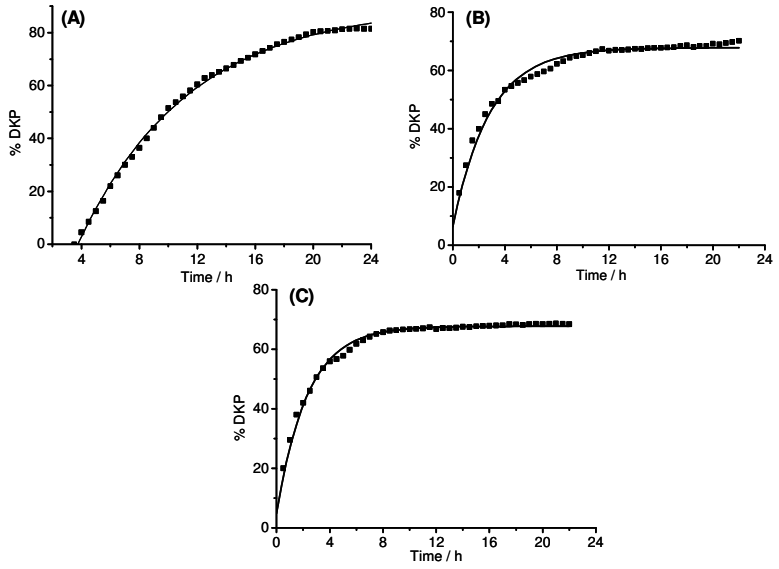

Figure 4.5 Time dependence of the formation of DKP for (A) aspartame, (B) [(η^6-*p*-cymene)Ru(η^6-aspartame)]$^{2+}$ (**3**) and (C) [(η^6-*p*-cymene)Os(η^6-aspartame)]$^{2+}$ (**4**) in 5% MeOD-d_4/5% D_2O/90% H_2O at 310 K in 10 mM phosphate buffer (pH 7.4), as determined by ^{1}H NMR spectroscopy. The curves represent the computer best-fits for first-order reactions with rate constants of 0.12 h^{-1} for aspartame (half life = 6.01 ± 0.56 h), 0.36 h^{-1} for **3** (half life = 1.95 ± 0.08 h)**,** and 0.43 h^{-1} for **4** (half life = 1.60 ± 0.05 h).

The major ESI-MS peaks observed from the NMR samples after 24 h at low cone voltage (10 V) were *m/z* 261.78, 646.53 and 735.54 for aspartame, **3** and **4**, respectively, consistent with the formation of DKP$^+$, [(η^6-*p*-cymene)Ru(η^6-DKP)](OTf)$^+$ and [(η^6-*p*-cymene)Os(η^6-DKP)](OTf)$^+$ (calcd *m/z* 262.10, 647.06, 747.12). The data for **3** and **4** are shown in Figure 4.6. The proposed pathway was thus confirmed, and the ESI-MS data eliminated the possibility that the observed NMR spectral changes were caused by hydrolysis of the ether bond. These results also illustrate the stability of the metal-arene bonds in these complexes since they remained intact throughout.

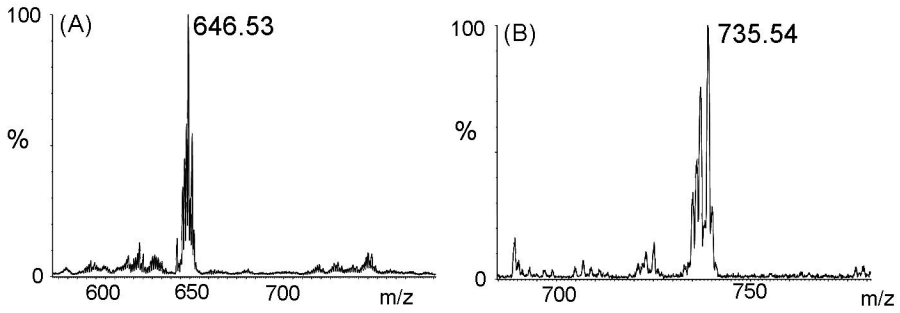

Figure 4.6 Characterisation of metal – DKP adducts. ESI mass spectra of solutions of (A) $[(\eta^6\text{-}p\text{-cymene})Ru(\eta^6\text{-aspartame})]^{2+}$ (**3**) and (B) $[(\eta^6\text{-}p\text{-cymene})Os(\eta^6\text{-aspartame})]^{2+}$ (**4**) in 5% MeOD-d_4/5% D_2O/90% H_2O after 24 h. Peaks at *m/z* 646.53 and 735.54 correspond to $\{[(\eta^6\text{-}p\text{-cymene})Ru(\eta^6\text{-DKP})](OTf)\}^+$ and $\{[(\eta^6\text{-}p\text{-cymene})Os(\eta^6\text{-DKP})](OTf)\}^+$ (calcd *m/z* 647.06, 737.12), respectively.

4.3.4 Electrochemical Behaviour

The redox properties of aspartame, **3** and **4** were investigated in the presence of 0.1 M tetrabutylammonium tetrafluoroborate ($TBABF_4$) as the supporting electrolyte in *N,N*-dimethylformamide (DMF).

The cyclic voltammogram of aspartame shows a quasi-reversible reduction peak at -1.133 V ($E_{1/2}$ = 0.946 V) at a scan rate of 0.1 Vs^{-1} (Figure 4.7). Due to the small amounts of material available, the more sensitive technique of differential pulse polaragraphy was used to investigate the ruthenium and osmium complexes. The introduction of a metal centre caused an increase in complexity of the redox behaviour, a shift in the reduction to less negative potentials, and a change in the reversibility of the process. Complex **3** exhibited a two-step reductive process at -0.377 V and -0.664 V, the latter showing a reverse wave at -0.643 V (Figure 4.8A).

Contrastingly, **4** was reduced in a single step at -0.619 V with a reverse wave at -0.177 V (Figure 4.8B). The large separation in the peaks for the osmium complex suggests that a chemical reaction follows reduction, most likely due to movement of the electrons within the system. Unfortunately, it was not possible to identify the products of these transformations.

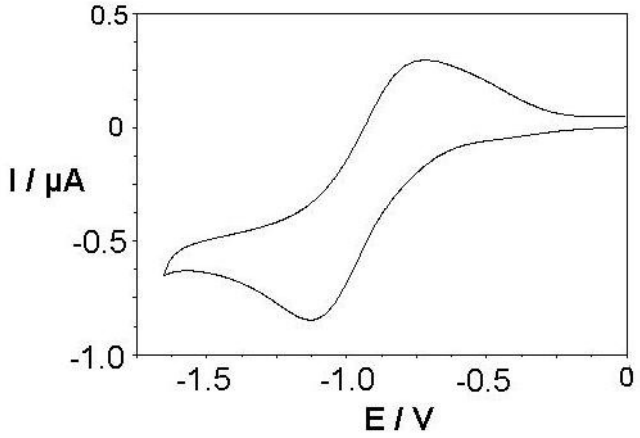

Figure 4.7 Cyclic voltammogram of aspartame in 0.1 M $TBABF_4$/DMF at a scan rate of 0.1 Vs^{-1} corresponding to a quasi-reversible reduction with $E_{1/2} = 0.946$ V.

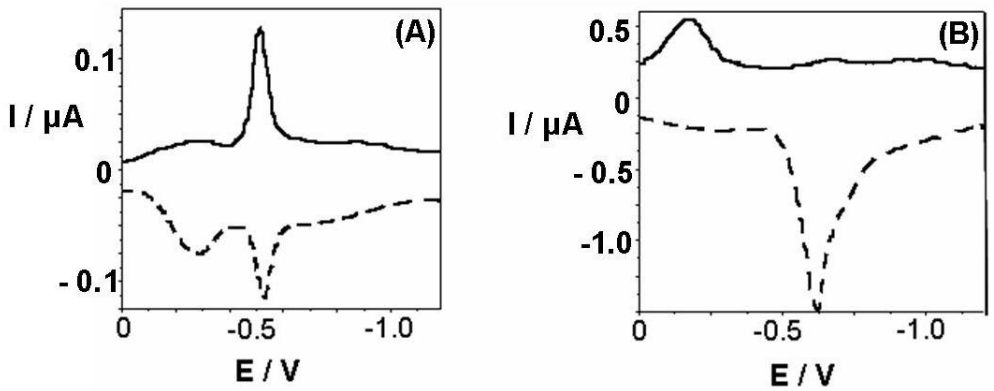

Figure 4.8 Forward (dashed line) and reverse (solid line) square-wave voltammograms of (A) [(η^6-*p*-cymene)Ru(η^6-aspartame)]$(OTf)_2$ (**3**) and (B) [(η^6-*p*-cymene)Os(η^6-aspartame)]$(OTf)_2$ (**4**) in 0.1 M $TBABF_4$/DMF**.**

The electrochemical reduction potentials indicate that only the ruthenium complex possesses redox activity within a biologically-relevant range of potentials (0 to – 0.5 V)[21]. ^{1}H NMR studies of reactions of the complexes with an excess of the biological reductant ascorbic acid (pK_a 4.2, ascorbate anion at physiological pH) were studied at 310 K in D_2O solutions containing 10 mM phosphate buffer (pH 7.04). Over a 24 h period, the only change observed in the ^{1}H NMR signals of aspartame and the osmium complex was the loss of bound OMe and growth of free MeOH peaks due to DKP formation. Contrastingly, many of the peaks corresponding to the ruthenium complex disappeared or changed appearance with time (Figure 4.9).

Kinetic data were derived by following changes in peak intensity, relative to an internal reference, for a number of different excess ascorbate concentrations (5-50 equivalents). The rate was found to be independent of the latter and the pseudo-first-order rate constant was determined to be *ca.* 6.9 x 10^{-5} s^{-1} (half-life 2.8 h; Figure 4.10). Unfortunately, full characterisation of the reaction mixture after 24 h was not possible by ^{1}H NMR spectroscopy, and mass spectrometry of the solution was inconclusive, suggesting that multiple products are forming, some of which may be unstable under such conditions.

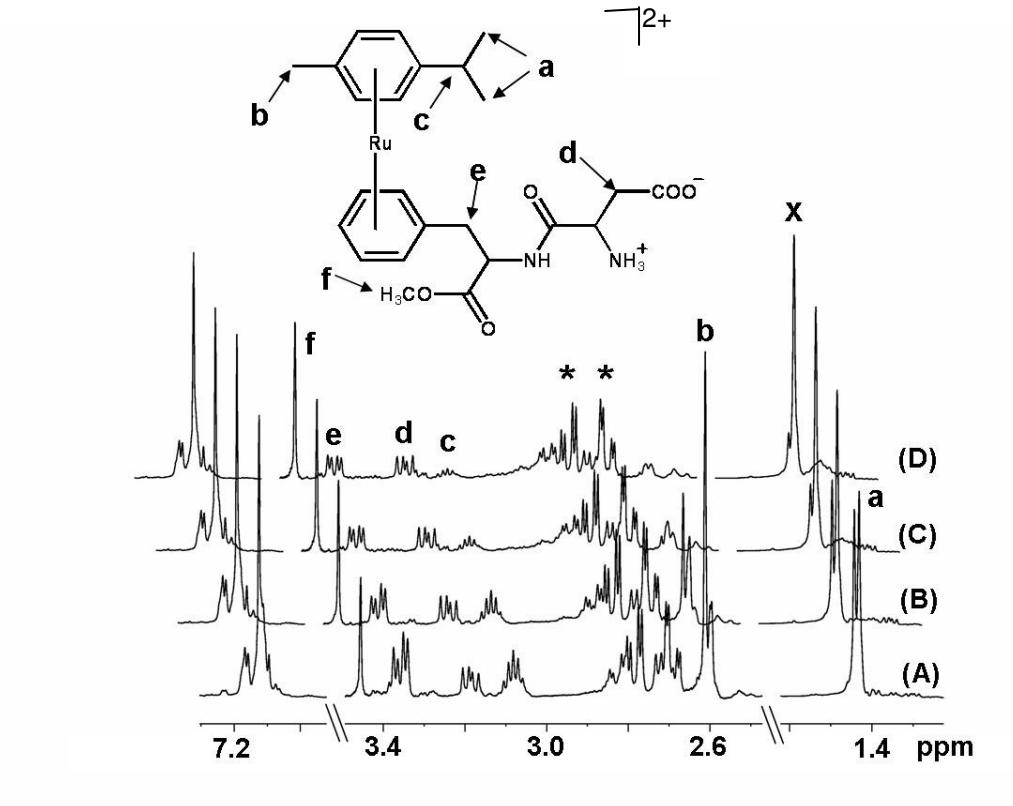

Figure 4.9 ^{1}H NMR spectra for the reaction of [(η^6-*p*-cymene)Ru(η^6-aspartame)](OTf)$_2$ (**3**) with ascorbate at pH 7.04, 310 K at times (A) 0 h, (B) 8 h, (C) 16 h and (D) 24 h, showing how the peaks for the aliphatic protons of the complex change with time. Peaks **b** – **e** decrease in intensity. Signals for all aromatic protons appear in the region between 7.1 ppm and 7.2 ppm, which decrease by *ca.* 35% over 24 h. Peaks corresponding to ascorbate are labelled (*). No new peaks appear over the timescale investigated. Peak **x** is unassigned.

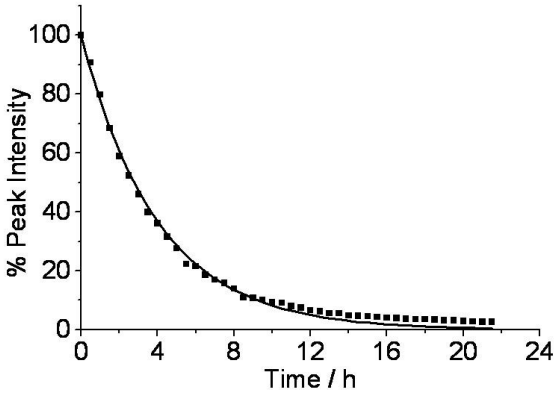

Figure 4.10 Decrease in intensity with time of signal at 3.08 ppm (**c**, Figure 4.9) of $[(\eta^6\text{-}p\text{-cymene})\text{Ru}(\eta^6\text{-aspartame})]^{2+}$ (**3**) (100 μM, 10 mM phosphate buffer, pH 7.04, D_2O, 310 K) after addition of 10 mol equivalents ascorbate. The curve represents the computer best-fit for a pseudo-first-order reaction with a rate constant of 6.9×10^{-5} s^{-1} (half-life 2.8 h).

4.3.5 Cytotoxicity

Complex **3** was non-toxic towards both the human ovarian A2780 and human lung A549 cancer cell lines at concentrations up to 100 μM, and therefore it is deemed inactive.

4.3.6 Interaction with Sweet Taste Receptor

Complexes **3** and **4** did not activate the sweet taste receptor up to concentrations of 1 mM (the highest test concentration). Furthermore, the inability of **3** to bind to the same receptor site as aspartame was illustrated by the absence of any competitive effects in the FLIPR assay response to aspartame in the presence of excess ruthenium

complex. The responses of aspartame and the metal complexes at 0.1 mM in the assay are shown in Figure 4.11 and that of aspartame with the ruthenium complex in Figure 4.12.

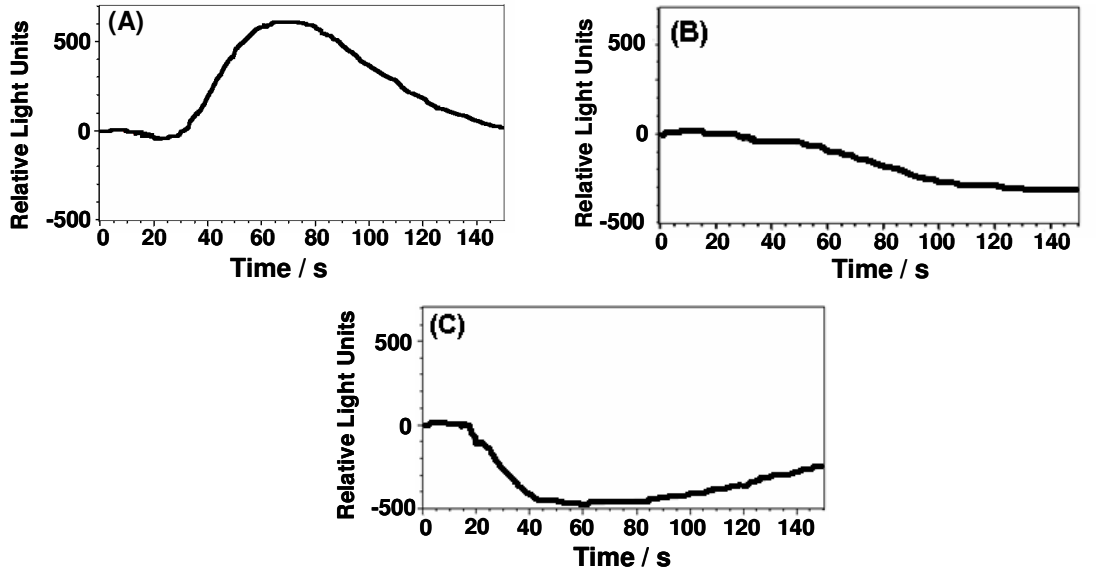

Figure 4.11 Time dependent Ca^{2+}-response of cells expressing the sweet taste receptor to application of (A) aspartame, (B) $[(\eta^6\text{-}p\text{-cymene})Ru(\eta^6\text{-aspartame})]^{2+}$ (**3**) and (C) $[(\eta^6\text{-}p\text{-cymene})Os(\eta^6\text{-aspartame})]^{2+}$ (**4**) (0.1 mM) recorded in the FLIPR assay. The increase in signal in (A) shows that aspartame stimulates the sweet taste receptor, whereas the metal complexes **3** and **4** are not able to stimulate the sweet taste receptor.

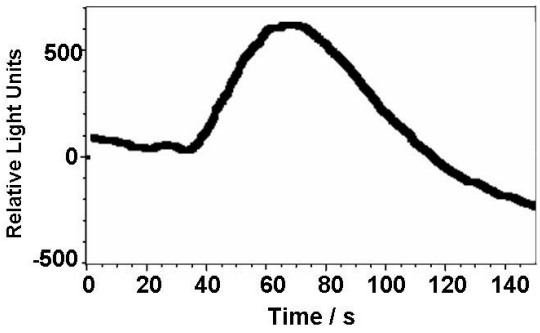
Relative Light Units
500
0
-500
0
20
40
60
80
100
120
140
Time / s

```
ERROR: stackunderflow
OFFENDING COMMAND: ~

STACK:
```